



## Measurements of Laminar and Turbulent Burning Velocities of N-Butanol/Air Mixtures at Elevated Temperatures and Pressures

Pervez Ahmed & Junfeng Yang

To cite this article: Pervez Ahmed & Junfeng Yang (18 Jul 2025): Measurements of Laminar and Turbulent Burning Velocities of N-Butanol/Air Mixtures at Elevated Temperatures and Pressures, Combustion Science and Technology, DOI: [10.1080/00102202.2025.2531539](https://doi.org/10.1080/00102202.2025.2531539)

To link to this article: <https://doi.org/10.1080/00102202.2025.2531539>



© 2025 The Author(s). Published with license by Taylor & Francis Group, LLC.



[View supplementary material](#)



Published online: 18 Jul 2025.



[Submit your article to this journal](#)



Article views: 40



[View related articles](#)



[View Crossmark data](#)

# Measurements of Laminar and Turbulent Burning Velocities of N-Butanol/Air Mixtures at Elevated Temperatures and Pressures

Pervez Ahmed\* and Junfeng Yang

School of Mechanical Engineering, University of Leeds, UK

## ABSTRACT

Experimental results of laminar burning velocities  $u_l$  and the associated flame front turbulent burning velocities  $u_{tr}$  and  $u_{tm}$  of premixed n-butanol air mixtures are measured inside a fan stirred combustion vessel, using high-speed Schlieren photography. Measurements were made between equivalence ratios from 0.7 to 1.4 at an initial temperature of 360 K and pressures ranging from 0.1 to 1.0 MPa. For turbulent studies, uniform and isotropic turbulence was created in the combustion vessel by four fans and turbulence rms velocities,  $u' = 0.5$  up to 6.0 m/s were obtained.  $u_l$ , and the associated parameters  $L_b$ ,  $Ma_{sr}$ ,  $Pe_{cl}$  and the corresponding  $K_{cl}$  associated with the onset of instabilities is presented.  $u_l$ , increased with  $\phi$  and reduced with increasing pressure while  $L_b$  decreased with increasing pressure and  $\phi$ .  $Ma_{sr}$  decreases with pressure and increasing  $\phi$ , with values becoming eventually negative at high pressures and rich mixtures. A satisfactory correlation exists between  $K_{cl}$  and  $Ma_{sr}$  with an  $R^2$  value of 0.859. Turbulent burning rates of n-butanol/air mixtures at high initial temperatures and up to 1.0 MPa in a controlled environment are reported for the first time.  $u_{tr}$ , values increase with increase in both  $\phi$  and  $u'$ . Increase in equivalence ratio and  $u'$  also enhanced  $u_{tr}$ .  $u_{tr}$  of n-butanol/air mixtures are higher than iso-octane/air mixtures which is attributed to lower  $Ma_{sr}$ . Dimensionless values of  $u_{tm}/u'_k$  decreased with increasing  $K$  for a given  $Ma_{sr}$ . However, for a constant  $K$ , decrease in  $Ma_{sr}$  lead to increased  $u_{tm}/u'_k$  values. The  $u_{tm}/u'_k$  curves from previous studies are extended to a positive  $Ma_{sr}$  of 10 along with the quench regime identified. It is envisaged that the current work facilitates a rich database that can aid in detailed chemical modelling or engine simulations using n-butanol as fuel.

## ARTICLE HISTORY

Received 22 May 2025

Revised 1 July 2025



Accepted 6 July 2025

## KEYWORDS


Experimental; laminar burning velocities; turbulent burning velocities; turbulent combustion; n-butanol

## Introduction

Emissions due to fossil fuels are a major contributor toward global warming and climate change crisis and hence alternative fuels are being sought to meet the energy supply demands (Veloo et al. 2010). Alcohol fuels have gained research attention in the recent past as promising alternative fuels potentially offering higher efficiency and minimum pollution (Beatrice, Bertoli, and Giacomo 1998; Demirbas 2007; Sarathy et al. 2009). Many countries have realised the importance of using alcohol fuels and have established

**CONTACT** Junfeng Yang  [J.Yang@leeds.ac.uk](mailto:J.Yang@leeds.ac.uk)  School of Mechanical Engineering, University of Leeds, Leeds, LS2 9JT, UK

\*Visiting Researcher, School of Mechanical Engineering, University of Leeds, Leeds, UK, LS2 9JT

 Supplemental data for this article can be accessed online at <https://doi.org/10.1080/00102202.2025.2531539>.

© 2025 The Author(s). Published with license by Taylor & Francis Group, LLC.

This is an Open Access article distributed under the terms of the Creative Commons Attribution License (<http://creativecommons.org/licenses/by/4.0/>), which permits unrestricted use, distribution, and reproduction in any medium, provided the original work is properly cited. The terms on which this article has been published allow the posting of the Accepted Manuscript in a repository by the author(s) or with their consent.

policies promoting its use (Oced 2011). These fuels are found to have high laminar flame speeds and high octane numbers which make them a better alternative option in engines. Oxygen content in alcohol fuels reduces CO and particulate emission as well (Karabektas and Hosoz 2009; Yacoub, Bata, and Gautam 1998). Among alcohol fuels, n-butanol has: low vapor pressure which reduces the chances of vapor lock (Serras-Pereira, Aleiferis, and Richardson 2013), less hygroscopic aiding transportation with the existing infrastructure, and has better fuel economy due to high energy density (Serras-Pereira, Aleiferis, and Richardson 2013) and is capable of operating in existing engines with either a little or no modification at all (Beatrice, Bertoli, and Giacomo 1998).

Fundamental studies of premixed n-butanol/air mixtures' laminar burning rates are investigated (Gu et al. 2009, 2010; Gu, Li, and Huang 2011; Katoch et al. 2019; Konnov 2010; Liu et al. 2014; Qin and Ju 2005; Sarathy et al. 2009; Simon 1951; Veloo et al. 2010; Zhang et al. 2008, 2018) in different experimental configurations. Many investigations involving n-butanol/gasoline blends and n-butanol/diesel blends on the efficiency of spark ignition engines have also been reported (Alasfour 1997a, 1997b; Bhattacharya, Chatterjee, and Mishra 2004; Chen et al. 2014; Gautam and Martin 2000; Gautam, Martin, and Carder 2000; Karabektas and Hosoz 2009; Serras-Pereira, Aleiferis, and Richardson 2013; Szwaja and Naber 2010; Yacoub, Bata, and Gautam 1998). Details of different research studies are tabulated in Table 1. While few studies are reported on the use of n-butanol as a fuel in engines, there is limited work reported on combustion of n-butanol in a controlled turbulent environment. It is also suggested in (Aleiferis, Serras-Pereira, and Richardson 2013) that data related to combustion of the alcohol fuels in controlled turbulent environments would reveal great details to improve the limitations in the current combustion diagrams. Therefore, the current experimental work aims to provide a fundamental understanding of laminar and turbulent combustion characteristics of n-butanol in a well-controlled combustion vessel at high initial temperature over a range of pressures and  $\phi$  for different turbulent velocities that replicate engine-like conditions. Values of turbulent burning velocities derived using other correlations are compared with the present experimental results and discussed. Dimensionless correlations of turbulent burning velocity normalised by the effective rms turbulent velocity,  $u_{tm}/u'_k$  are presented in terms of  $K$ , for different  $Ma_{sr}$ . The  $u_{tm}/u'_k$  curves from previous studies are extended to a positive  $Ma_{sr}$  of 10 and the associated quench regime is identified. The authors believe that the current work provides a rich database of n-butanol mixture burning rates that can aid in detailed chemical modelling or engine simulations.

## Laminar burning velocity, $u_l$

Fundamental understanding of laminar burning velocity,  $u_l$ , is key in developing novel and improved combustion engines. It is also required to determine the pressure and temperature dependencies of both laminar (Van Lipzig et al. 2011) and turbulent flames. It also plays an important role in turbulent combustion simulation and validation of chemical kinetic mechanisms (Li et al. 2015). The influence of flame chemistry on turbulent premixed flames is usually expressed through  $u_l$  in laminar flamelet models, and Markstein numbers (Bradley et al. 1998; Bradley, Gaskell, and Gu 1996; Linan and Williams 1993). It is well known that laminar and turbulent burning velocities are significantly affected by flame

**Table 1.** Research studies involving n-butanol as a fuel.

Authors	Configuration	Fuel Mixtures	Initial Conditions	Remarks/Conclusions
Gu et al. (2009)	Spherically expanding laminar flames	n-butanol/air	0.1–0.25 MPa, 413–473K	$u_f$ increase with temperature and decrease with initial pressure.
Veloo and Egolfopoulos (2011)	Counter flow laminar flames	n-butanol isotherms	1 atm, 343K	Among all isomers n-butanol exhibited the highest flame speeds.
Zhang et al. (2013) and Broustail et al. (2011)	Spherically expanding laminar flames	n-butanol/iso-octane and ethanol/iso-octane	0.1 MPa and 393K	$u_f$ of n-butanol are higher than iso-octane but less than ethanol. Flame speeds are enhanced with increasing blending ratio of n-butanol.
Broustail et al. (2013)	Spherically expanding laminar flames	n-butanol/iso-octane and ethanol/iso-octane	0.1–1.0 MPa and 423K	Difference in $u_f$ for alcohol fuels and iso-octane are minimal with increase in initial pressures.
Zhang et al. (2018)	Spherically expanding laminar flames	acetone, butanol and ethanol (ABE) mixtures	0.1 MPa, 358–428K	$u_f$ of ABE mixtures are closer to n-butanol.
Beeckmann et al. (2009, 2010 and 2014)	Spherically expanding laminar flames	Methanol, Ethanol, n-propanol, n-butanol, iso-octane	1.0 MPa	Present numerical models for n-butanol under predict the experimentally measured values at high pressures.
Wu and Law (2013)	Spherically expanding laminar flames	n-butanol isotherms	353–373K, 1–5 atm	n-butanol exhibited high $u_f$ values among all isotherms. These findings corroborated with their computational study. The reduction in $u_f$ for other isotherms was attributed to the branching of intermediate species forming more stable compounds.
Alasfour (1997a)	Single cylinder engine	n-butanol/gasoline blends	308K	Reported a reduction in output power compared to engines fuelled with pure gasoline.
Yao et al. (2010)	Diesel engine	n-butanol/diesel fuel	313±3K	n-butanol addition improves soot and CO emissions significantly without compromising on the break specific fuel consumption.
Chen et al. (2014)	single-cylinder research engine	n-butanol/diesel ratio blends	0.18 MPa, 298K	Their results show that high butanol/diesel ratio blend with medium exhaust gas recirculation (EGR) can potentially achieve ultra-low NOx and soot emissions while maintaining high thermal efficiencies.
Szwaja and Naber (2010)	sparkd ignited IC engine	n-butanol and gasoline blends	303K	n-butanol has the potential to perform as a direct substitute for gasoline either as a pure fuel or blended with gasoline because of the similar thermo-physical properties.
Valentino et al. (2012) Merola et al. (2011) Serras-Pereira, Aleiferis, and Richardson (2013)	Diesel Engine Spark Ignition engines Direct-injection spark-ignition	n-butanol/diesel butanol/gasoline C2–C4 alcohols with iso-oct and gasoline	295–311K 293–363K	n-butanol and ethanol fuels burn faster than gasoline and iso-octane at higher temperatures. Their findings suggested that alcohol fuels at lean conditions were robust in combustion stability than hydrocarbons.
Aleiferis, Serras-Pereira, and Richardson (2013)	Spark ignition engine, Optical study/ Turbulent	n-butanol, ethanol, iso-octane and methane	0.5 bar	n-butanol and ethanol have comparable burning rates while iso-octane reported the slowest. It was suggested that combustion of these fuels in controlled turbulent environments would reveal great details to improve the current combustion diagrams.

(Continued)

**Table 1.** (Continued).

Authors	Configuration	Fuel Mixtures	Initial Conditions	Remarks/Conclusions
Siwale et al. (2013)	Diesel Engine	n-butanol/diesel	298K	Increase in the butanol blend ratio significantly improves the reduction of emissions.
Katoch et al. (2019)	Planar stabilised flames	n-butanol/air	350–600K	The variation of temperature exponent ( $\alpha$ ) with equivalence ratio ( $\Phi$ ) was reported also for the first time. The values exhibit a non-linear inverted parabolic profile with a minimum value occurring for slightly rich mixtures at $\Phi = 1.1$

stretch (Bagdanavicius et al. 2015; Bradley, Gaskell, and Gu 1996). The total stretch rate,  $\alpha$ , for a spherically expanding flame is a function of  $r_u$  and  $S_n$  (Bradley et al. 1998)

$$\alpha = \frac{1}{A_f} \frac{dA_f}{dt} = \frac{2}{r_u} \frac{dr_u}{dt} = \frac{2}{r_u} S_n. \quad (1)$$

Here,  $A_f$  is the flame surface area,  $t$  is the time,  $r_u$  is the radius of the cold front of the flame and  $S_n$  is the stretched flame speed. Spherical flames are stretched due to both curvature and strain rate (Gu et al. 2000).

The effect of stretch on  $u_l$  is given by

$$u_l - u_n = L_c \alpha_c + L_s \alpha_s. \quad (2)$$

Here  $\alpha_c$  and  $\alpha_s$  are the stretch rates related to flame curvature and flow field strain, while  $L_c$  and  $L_s$  are the associated Markstein lengths (Bradley, Gaskell, and Gu 1996).  $u_l$  and  $u_n$  are the unstretched and stretched laminar burning velocity, respectively.  $r_u$  is related to the cold flame front radius, defined as the isotherm that is 5K above the reactant temperature, observed by Schlieren cine photography,  $r_{sch}$  by

$$r_u = r_{sch} + 1.95 \delta_l \left( \frac{\rho_u}{\rho_b} \right)^{0.5} \quad (3)$$

Here  $\rho_u$  is the density of the unburned and  $\rho_b$  that of the burned gas at the adiabatic flame temperature and  $\delta_l$  is the laminar flame thickness ( $= \nu/u_l$ ). Where  $\nu$  is the kinematic viscosity of the unburned mixture.  $S_n$  is related to  $r_u$  and  $u_n$  as (Bradley et al. 1998)

$$S_n = \frac{dr_u}{dt} \quad (4)$$

The influence of total stretch,  $\alpha$ , on  $S_n$  is given by

$$S_s - S_n = L_b \alpha \quad (5)$$

Where  $L_b$  is the burned gas Markstein length (Clavin 1985) and  $S_s$  is the unstretched flame speed.  $S_s$  is obtained from the extrapolation of  $S_n$  to the zero stretch ( $\alpha = 0$ ) in the  $S_n$  vs.  $\alpha$  curve. For cellular flames  $S_s$  is obtained by extrapolating the part of the  $S_n$  curve before the onset of cellularity. Markstein lengths express the reduction in burning velocity due to stretching. The gradient of the best straight-line fit to the experimental data in the  $S_n$  vs.  $\alpha$  curve gives  $L_b$ . The strain rate Markstein length,

$L_{sr}$ , and Markstein number related to strain rate,  $Ma_{sr}$ , are measured directly from the stretched laminar flame measurements, with the influence of straining directly related to strain rate by (Bradley, Gaskell, and Gu 1998; Haq et al. 2002).

$$L_{sr} = \frac{1}{\rho_u/\rho_b - 1} (L_b - L_s) \quad (6)$$

$$Ma_{sr} = \frac{L_{sr}}{\delta_l} \quad (7)$$

The parameter  $L_s$  is obtained using multiple regression analysis (Bradley, Gaskell, and Gu 1996),  $u_l$ , is deduced from  $S_s$  using the relation (Bradley et al. 1998):

$$u_l = S_s \frac{\rho_b}{\rho_u}. \quad (8)$$

However, in recent studies (Bonhomme, Selle, and Poinso 2013; Bradley, Lawes, and Morsy 2019), it is shown that for hydrocarbons like iso-octane and n-butanol flames, the mean burnt gases temperature,  $T_b$ , is not equal to the adiabatic temperature,  $T_{ad}$  due to  $T_{ad}$  being influenced by stretch and Lewis number,  $Le$ . This effect is shown in (Bonhomme, Selle, and Poinso 2013; Chung et al. 1986; Clavin and Williams 1982) as

$$\frac{T_b - T_{ad}}{T_{ad}} = \left( \frac{1}{Le} - 1 \right) \frac{D}{u_l} \alpha \quad (9)$$

$Le$  is the Lewis number of the limiting reactant,  $D$ , is the thermal diffusivity of the mixture. The effect of  $T_b < T_{ad}$ , results in the mean burned gas density  $\bar{\rho}_b$  to be greater than the adiabatic burned gas density,  $\rho_b$  i.e.  $\bar{\rho}_b > \rho_b$ . Therefore, to include the effect of  $Le$  and  $\alpha$  upon  $u_l$ , in the present study it is calculated using the equation

$$u_l = S_s \frac{\bar{\rho}_b}{\rho_u}. \quad (10)$$

These densities,  $\bar{\rho}_b$ ,  $\rho_u$ , and thermal diffusivity,  $D$ , of the mixture were obtained from the thermal equilibrium program GasEq, developed by (Morley 2005).

### Turbulent burning velocity, $u_{tr}$

Many correlations exist in the literature to calculate turbulent burning velocities (Bagdanavicius et al. 2015; Bradley et al. 2003, 2013; Bradley, Lawes, and Mansour 2009a, 2011; Kobayashi, Kawabata, and Maruta 1998; Kolla et al. 2009; Kolla, Rogerson, and Swaminathan 2010; Lipatnikov and Chomiak 2002). Bradley et al. (2003) measured turbulent burning velocities associated with different surfaces using techniques like Schlieren photography and Mie-scattering. Turbulent burning velocity,  $u_{tr}$ , is associated with mean radius of Schlieren front,  $r_{sch}$ , while turbulent burning velocity  $u_{tv}$  is obtained from the mean radius,  $r_v$ , of Mie-scatter image. However, Schlieren imaging technique is more convenient and avoids the complexity of using class 4 lasers as in Mie scattering technique to derive turbulent burning velocities. In their work (Bradley et al. 2003) it was shown that there exists a linear relationship between,  $u_{tr}$  and  $u_{tv}$  whose gradient yields an expression for  $u_{tr}$  given by

$$u_{tv} = u_{tr} = 0.9 \frac{\rho_b}{\rho_u} \frac{dr_{sch}}{dt}. \quad (11)$$

However, in order to include the effect of  $Le$  and  $\alpha$  in the present study, Equation 11 was modified to

$$u_{tv} = u_{tr} = 0.9 \frac{\bar{\rho}_b}{\rho_u} \frac{dr_{sch}}{dt}. \quad (12)$$

For comparing any measured turbulent burning velocities, say  $u_{tr}$ , using the existing correlations, characteristics such as  $u_l$ ,  $\delta_l$  and turbulent characteristics like  $u'$  and turbulent length scales must be known (Lawes et al. 2012). The Taylor scales,  $\lambda$ , and Kolmogorov scales,  $\eta$ , are calculated using the relations given by (Mccomb 1990):

$$R_\lambda = u_l \lambda / \nu, \quad (13)$$

Where  $R_\lambda$  is the Taylor scale Reynolds number with  $\nu$  the kinematic viscosity and

$$\frac{\lambda}{L} = \frac{A}{R_\lambda'} \quad (14)$$

Here  $A$  is a numerical constant,  $A = 16 \pm 1.5$  (Mccomb 1990).

The Kolmogorov scale,  $\eta$ , is calculated using the relation (Mccomb 1990)

$$\eta = \frac{\lambda}{15^{0.25} R_\lambda^{0.5}} \quad (15)$$

The turbulent Reynolds number ( $R_L$ ) based on the integral length scale,  $L$ , is defined as

$$R_L = \frac{u' L}{\nu} \quad (16)$$

The value of turbulent Reynolds number ( $R_L$ ) inside Leeds MK-II vessel is in the range of 1,600–10,000 depending on the fan rotating speed (1,000–6,000 rpm) (Morsy 2019).

The ratio of chemical lifetime,  $\delta_l/u_l$ , to eddy lifetime,  $\lambda/u'$ , is the Karlovitz stretch factor,  $K$ , and is given by (Bray 1996; Chakraborty and Cant 2006)

$$K = \frac{\delta_l/u_l}{\lambda/u'} \quad (17)$$

With  $\delta_l = \nu/u_l$ , and  $A = 16$ ,  $K$  is given by (Bradley et al. 2005)

$$K = 0.25 \left( \frac{u'}{u_l} \right)^2 R_L^{-0.5} \quad (18)$$

During the early stage of flame-kernel growth, only the smallest turbulence wavelengths are affecting the surface structure and the effective rms turbulent velocity,  $u'_k$ , that acting on the flame is less than the rms velocity,  $u'$ , that is measured in the vessel in the absence of any flame. As the flame propagates, it becomes more susceptible to the full range of turbulence scales present and  $u'_k$  increases until approaches  $u'$  (Bradley, Lawes, and Mansour 2011). Hence, the effective rms turbulent velocity,  $u'_k$ , is introduced as a primary requirement to derive turbulent burning velocities at a given  $u'$ .

The details of calculating  $u'_k$  over a range of wavelengths is presented in (Bradley, Lawes, and Mansour 2011). The behaviour of  $u'_k/u'$  during spherical flame propagation is derived by integration of the entire power spectral density,  $\bar{S}(\bar{k}_\eta)$ , over the entire range of wavelengths as (Abdel-Gayed, Bradley, and Lawes 1987; Bradley, Lawes, and Mansour 2009b)

$$\frac{u'_k}{u'} = \left[ \frac{15^{0.5} \bar{k}_{\eta 2}}{R_\lambda} \int_{\bar{k}_{\eta 1}} \bar{S}(\bar{k}_\eta) d\bar{k}_\eta \right]^{0.5} \quad (19)$$

$$\bar{S}(\bar{k}_\eta) = \frac{0.01668 R_\lambda^{2.5} + 3.74 R_\lambda^{0.9} - 70 R_\lambda^{-0.1}}{1 + (0.127 R_\lambda^{1.5} \bar{k}_\eta)^{5/3} + (1.15 R_\lambda^{0.622} \bar{k}_\eta)^4 + (1.27 R_\lambda^{0.357} \bar{k}_\eta)^7} \quad (20)$$

$\bar{k}_\eta$  is a dimensionless wavenumber, defined as  $2\pi/\text{wavelength}$  multiplied by  $\eta$ . The lower and upper limits  $\bar{k}_{\eta 1}$  and  $\bar{k}_{\eta 2}$  respectively are the associated largest and the smallest possible wavelengths evaluated using the general wave number,  $\bar{k}_{\eta k}$  given by

$$\bar{k}_{\eta k} = \frac{2\pi\eta}{n_k L} = \left( \frac{32\pi}{15^{0.25} n_k} \right) R_\lambda^{-1.5} \quad (21)$$

Here  $n_k$  is defined as  $n_k = 2r_{0.5}/L$ , where  $r_{0.5}$  is the mean radius of the flame. Typical curves of  $u'_k/u'$  plotted against increasing  $n_k$  are shown in Figure 1 for the  $R_\lambda$  values, associated with the current  $R_L$  and  $u'$  values employed in this study. The maximum value of  $u'_k/u' = 0.81$  is found to be at a value of  $n_k > 6$ . It is suggested in (Bradley, Lawes, and Mansour 2011) that a value of  $n_k = 2$  corresponds to the onset of developed linear regime for a non-quenching flame. Therefore, for flame analysis at a value of  $n_k$  above 2 we should quantify the present experimental results.

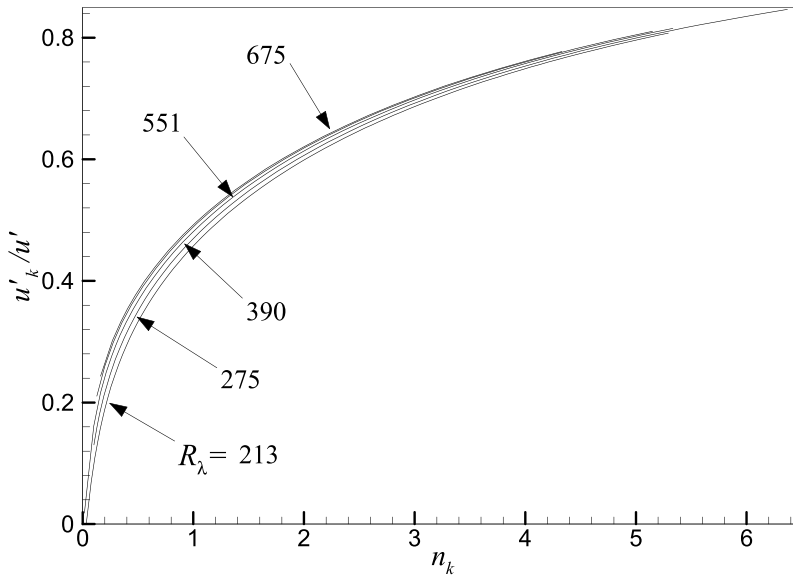


**Figure 1.** Variation of  $u'_k/u'$  with increasing  $n_k$  for different  $R_\lambda$ .



## Experimental method

Experimental measurements are carried out in a 30-liter spherical vessel, of 380 mm internal diameter with three pairs of orthogonal windows that are 100 mm and 150 mm in diameter (Lawes et al. 2012). Once the combustion vessel was ready and vacuumed, the liquid *n*-butanol was added through the appropriate needle valve by monitoring the pressure on the digital static pressure gauge. The vessel was again filled with dry air up to the required initial pressure for explosion. Turbulence is generated by four identical, eight bladed fans, each driven by an independently controlled 8 kW electric motor with accuracy within  $\pm 5\%$  of the set speed. The mean and rms turbulent velocities, and the associated integral length scales have been determined using laser Doppler velocimetry (Bradley, Gaskell, and Gu 1996). More recently, the spatial and temporal distributions of the turbulence fluctuations have been investigated in (Bradley, Lawes, and Morsy 2021) using particle image velocity (PIV). Uniform and isotropic turbulence is reported in the central region (150 mm diameter) of the vessel (Bradley, Lawes, and Morsy 2019, 2021; Nwagwe et al. 2000). The flow uniformity is particularly good up to 50 mm radii from the center with fluctuations within 10% of the mean velocity. It is reported in (Bradley, Lawes, and Morsy 2021) that the uniform turbulent zone is limited to 40 mm radii at fan speeds  $>6000$  rpm ( $u' = 6$  m/s). Nonetheless, the current data analysis was conducted at flame radii of 30 mm where turbulence is isotropic and uniform regardless of fan speed. The integral length scale is found to be 20 mm (Bradley, Lawes, and Morsy 2021), and is independent of the fan speed between 1000 and 10,000 rpm, except at 500 rpm where it was found to be 24 mm.  $u'$ , is given by

$$u'(m/s) = 0.00119f_s(rpm) \quad (22)$$

where  $f_s$  is the fan speed. It is reported in (Morsy 2019) that the impact of both temperature and pressure on the rms velocity,  $u'$ , is  $<12\%$  at the highest fan speeds employed. Consequently, at  $p = 0.1$  MPa, the integral length scales are increased up to 10%, at initial temperatures of 400K while the impact of increasing pressure, at 300K, up to 1.0 MPa was found negligible. The changes in the turbulence characteristics are within the experimental measurement uncertainties and do not significantly impact the current analysis.

The initial mixture gas temperature is measured using a sheathed chromel–alumel K-type thermocouple, inside the chamber. A static piezoresistive pressure transducer is employed to measure the pressure during mixture preparation. This transducer is situated outside the vessel and was isolated just prior to ignition. A central spark plug with ignition energies of about 23 mJ (Nwagwe et al. 2000) was supplied from a 12 V transistorised automotive ignition coil (Bradley, Lawes, and Mansour 2011). All burning velocities are measured at sufficiently large radii so that spark effects could be neglected (Bradley et al. 1998). The fans were run during mixture preparation, both to ensure full mixing and to assist uniform heat transfer. For laminar studies the fans were switched off for a period of 20 s, following mixture preparation, before ignition. In turbulent tests the fans were maintained at the set speed, to produce the desired rms turbulence intensity throughout the mixture preparation, ignition and combustion period.

High-speed Schlieren photography was used to capture flame images at the rate of 5400 frames per second with a pixel resolution of 768x768. For each explosion flame radius was measured as a function of time. The process of identifying the flame radius for laminar

**Table 2.** Summary of experimental conditions at  $T_i = 360$  K,  $q$  indicates flame quenching.

P		0.1 MPa					0.5 MPa					1.0 MPa				
$\phi$		$u' (m/s)$					$u' (m/s)$					$u' (m/s)$				
0.7	0.5	1	2q	–	–		0.5	1	2q	–	–	0.5	1q	–	–	–
0.8	0.5	1	2	4q	6q		0.5	1	2	4	6	0.5	1	2	4	6
1.0	0.5	1	2	4	6		0.5	1	2	4	6	–	1	2	4	6
1.2	0.5	1	2	4	6		0.5	1	2	4	6	–	–	–	–	–
1.4	0.5	1	2	4	6		0.5	1	2	4	6	–	–	–	–	–

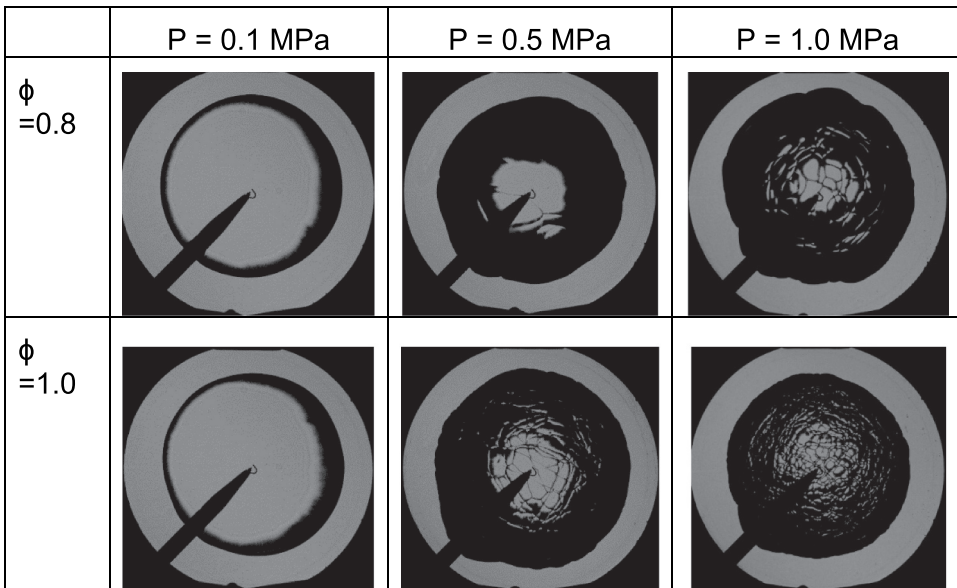
flames using level set technique is given in (Sethian 1999; Tripathi 2012). The details of measuring Flame speeds, laminar burning velocities, Markstein lengths and Markstein numbers are reported in (Bradley et al. 1998; Bradley, Gaskell, and Gu 1996).  $Ma_{sr}$  is obtained by dividing  $L_{sr}$  with the corresponding  $\delta_l$ . The calculation of  $u_l$  requires thermal expansion factor, which is the ratio of  $\bar{\rho}_b$  and  $\rho_u$ .

## Results

In this section,  $u_l$  of n-butanol/air mixtures are presented first followed by its turbulent burning characteristics over the range of conditions presented in Table 2.

### Laminar burning velocities, $u_l$

Typical laminar flame images at two different  $\phi$  and with increasing pressure at similar radius values are shown in Figure 2. Flame radius from these Schlieren images,  $r_{sch}$ , are

**Figure 2.** Laminar flame images at  $\phi=0.8$  and 1.0 at increasing initial pressure.

derived which are used to calculate  $r_u$  using Equation 3. Smooth flame propagation is observed at lower initial pressures, while at increased initial pressures flames develop cracks from the spark discharge, seen at 0.5 MPa and  $\phi = 0.8$ , as it progresses. These cracks lose their self-similarity as they grow and further cracks eventually become cellular at larger radii. As the initial pressure increases, the onset of cellularity begins at a relatively smaller radius.

Stretched flame speed,  $S_n$ , calculated using Equation 4, against  $\alpha$ , calculated using Equation 1, for initial pressures of 0.1, 0.5 MPa over the range of  $\phi=0.7$  to 1.4 are shown in Figures 3 and 4 respectively. Flame speeds of up to  $\phi=0.8$  at 1.0 MPa are shown in Figure 5. The solid lines in each case show the extrapolation of smooth stretched flame speed, independent of spark effect and cellularity, to zero stretch to obtain  $S_s$ .  $u_l$  was then calculated, using Equation 8 (Bradley et al. 1998).

Laminar burning velocity,  $u_l$ , of n-butanol/air mixtures are plotted against  $\phi$  at different initial pressures of 0.1, 0.5 and 1.0 MPa in Figure 6. Shown in Table 3 are the  $Le$  values used to calculate  $T_b$  and  $\bar{\rho}_b$  and these are taken from (Li, Jin, and Huang 2016). Mean values of  $u_l$  were obtained using three identical explosions at each experimental condition and are shown as filled symbols. The error bars denote the standard deviation and the solid line shows the best line fit through each set of data. Measurements could not be made for values of  $\phi$  greater than 0.8 at 1.0 MPa as not all the fuel was evaporated at this pressure and temperature of 360K. This limiting value of  $\phi$  is indicated by asterisk symbol in the figure.  $u_l$  decreased with increasing pressure. Values from other studies (Broustail et al. 2011; Sarathy et al. 2009; Veloo and Egolfopoulos 2011; Wang et al. 2018; Wu and Law 2013; Zhang et al. 2018) are also presented for the purpose of comparison. An increase in  $\phi$  leads to an increase in  $u_l$ .  $u_l$  values are observed to be the lowest for lean mixtures,  $\phi = 0.7$ . For a given pressure, peak values of  $u_l$  are observed on the richer side,  $\phi = 1.1$ . This is in line with the results

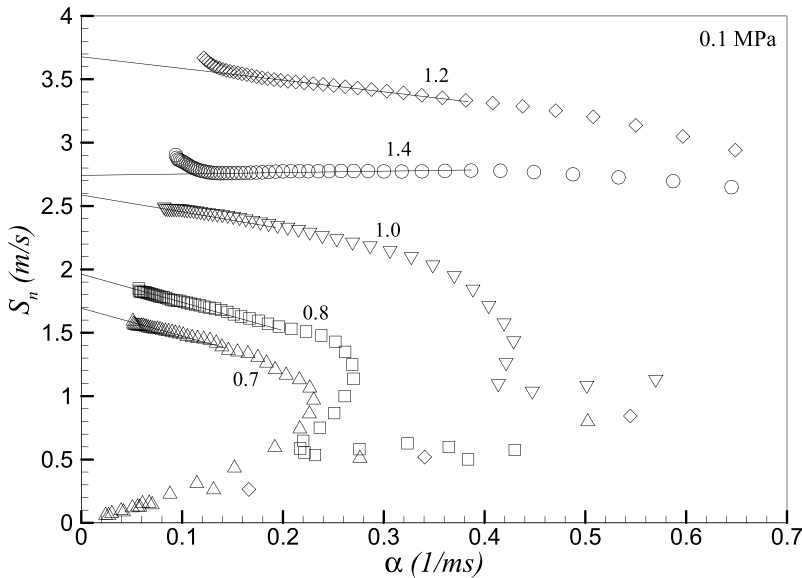


**Figure 3.** Stretched flame speed,  $S_n$ , against flame stretch  $\alpha$ , for different  $\phi$  at 0.1 MPa and 360 K.

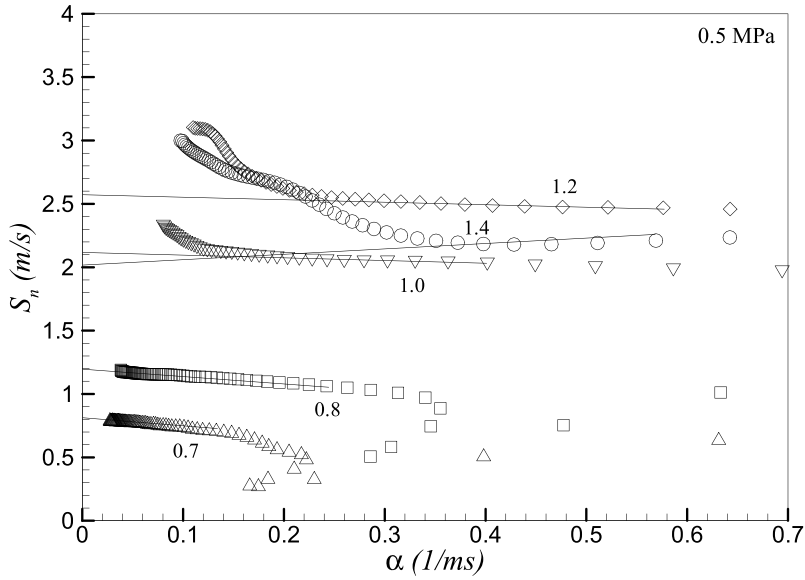


**Figure 4.** Stretched flame speed,  $S_n$ , against flame stretch  $\alpha$ , for different  $\phi$  at 0.5 MPa and 360 K.

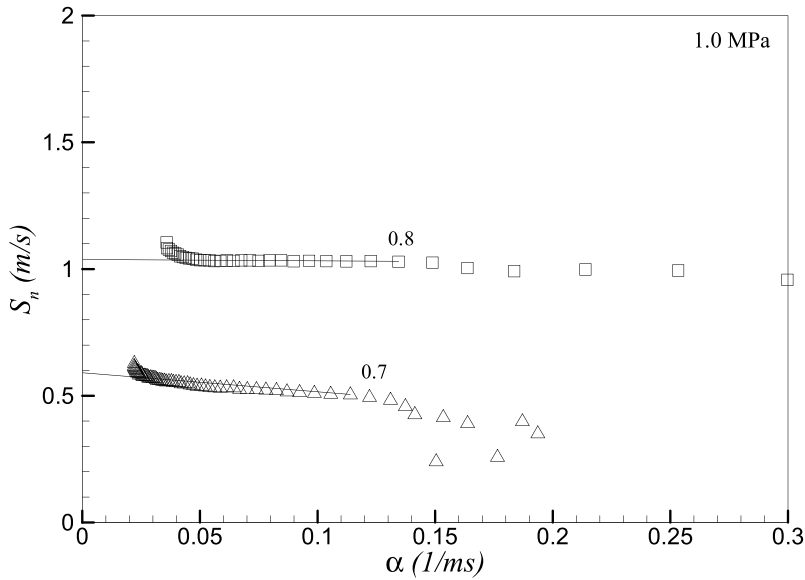


**Figure 5.** Stretched flame speed,  $S_n$ , against flame stretch  $\alpha$ , for different  $\phi$  at 1.0 MPa and 360 K.

reported in (Konnov 2010) and (Katoch et al. 2019). Despite similar conditions adopted by Wu and Law (Wu and Law 2013), which are close to the present work within the measurement uncertainty, a good agreement is seen on the lean-to-stoichiometric conditions; however, the rich side indicates some discrepancy of up to 8% higher values for the current measurements. This can be attributed to values of  $\bar{\rho}_b$  approaching those of  $\rho_b$  with increasing  $\phi$ , as a result of both the more rapid attainment of equilibrium,

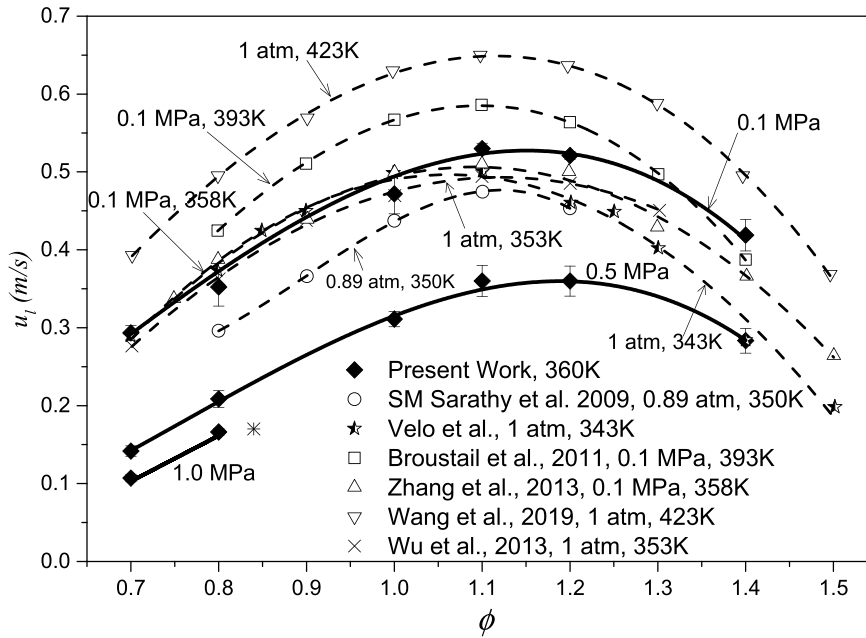


**Figure 6.** Unstretched laminar burning velocity,  $u_l$ , of n-butanol/air mixtures at 0.1, 0.5 and 1.0 MPa at 360 K.

**Table 3.** Lewis numbers of n-butanol/air mixtures from previous studies.

$\phi$	0.1 MPa, 433K, Zhang et al. (2013)	0.1 MPa, 363K, Li, Jin, and Huang (2016)	413K, Gu et al. (2009)	428K, Gu et al. (2010)
0.8	2.11	2.06	2.14	2.14
0.9	2.09		2.11	2.11
1.1	0.90			0.92
1.2	0.88	0.88	0.92	0.91
1.3	0.89		0.91	
1.4	0.87		0.90	
1.5	0.86	0.85	0.89	

and the decreasing values of  $Le$ . This indicates the level of scatter one should account for while designing the relevant combustion systems.

Shown in [Figure 7](#) are the corresponding  $L_b$  values derived from the region of stable flame propagation, independent of spark effect and cellularity.  $L_b$  are found to decrease with increasing pressure and also with increasing  $\phi$ . For a given  $\phi$ ,  $u_l$  values decrease with increasing pressure as the sensitivity to stretch (low  $L_b$  values) decreases causing the flame to become cellular at even smaller radii. An increase in hydrodynamic and thermo-diffusive instability at high initial pressures causes flame cellularity (Bradley et al. 2019). Consequently, the flame speeds increase drastically at the onset of cellularity causing the flame to burn more rapidly with increased flame surface area.

The rate of decrease in  $u_l$  reduces with increase in initial pressure from 0.5 to 1.0 MPa. At 0.5 MPa and rich mixtures,  $L_b$  values were negative which indicates an increase in burning rate with stretch. A decrease in  $L_b$  with pressure indicates a decrease in flame sensitivity to stretch and therefore reduces the  $u_l$  during the stable flame regime. As the flame reaches the

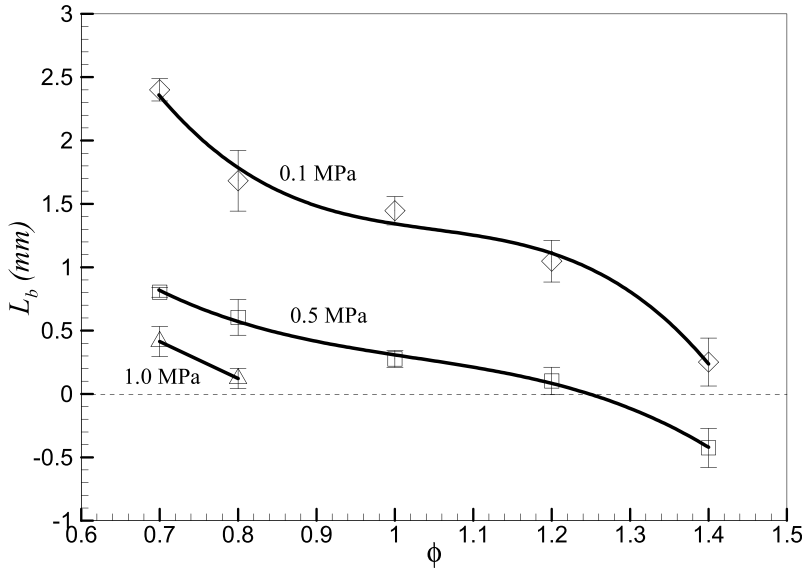
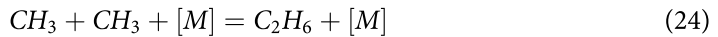
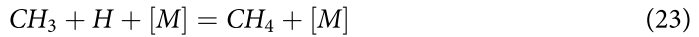


**Figure 7.** Markstein length,  $L_b$  (mm), of n-butanol/air mixtures at 0.1, 0.5 and 1.0 MPa at 360 K.

critical stretch, the flame becomes unstable and cellular and therefore cannot be used to calculate  $u_l$ . It is reported in (Liu et al. 2014), that the H and OH radicals, largely responsible for promoting fuel consumption and associated with increased flame speeds, drop significantly with increasing pressure; while marginal changes in  $\text{CH}_3$  and  $\text{C}_3\text{H}_6$  radicals are seen.  $\text{C}_3\text{H}_6$  has less reactivity among *alkene*. hydrocarbons [10], and the  $\text{CH}_3$  would promote chain termination through reactions R1 and R2, reducing the reactivity of fuel-air combustion system (Ranzi et al. 2012; Veloo et al. 2010). Thus, reducing  $u_l$  at higher pressures. However, the detailed reaction mechanism investigation remains out of the present work's scope.



$Ma_{sr}$ , at different pressures and  $\phi$  are shown in Figure 8. The process of deriving  $Ma_{sr}$  is again given in (Bradley, Gaskell, and Gu 1996). Values of  $\delta_l$ , were found using  $\delta_l = \nu/u_l$ . Values of  $\nu$ , are obtained from GasEq code (Morley 2005). Each open symbol represents a mean value of  $Ma_{sr}$  from three identical explosions, and the error bar shows the associated uncertainty in predicting the values which is likely to increase at higher pressures and at higher  $\phi$  due to the early development of onset of cellularity in the explosion flames, consequently reducing the regime of stable flame propagation. A significant decrease in the  $Ma_{sr}$  values are observed with an increase in  $\phi$  with values eventually reaching negative at high pressures. A decrease in  $Ma_{sr}$  is associated with an increased propensity for flame cellularity while limiting the stable flame regime for  $u_l$  deduction (Bradley et al. 2007). Nonetheless,  $u_l$  and the corresponding  $Ma_{sr}$  values provide useful datum to derive realistic mass burning velocities within the stable flame regime.

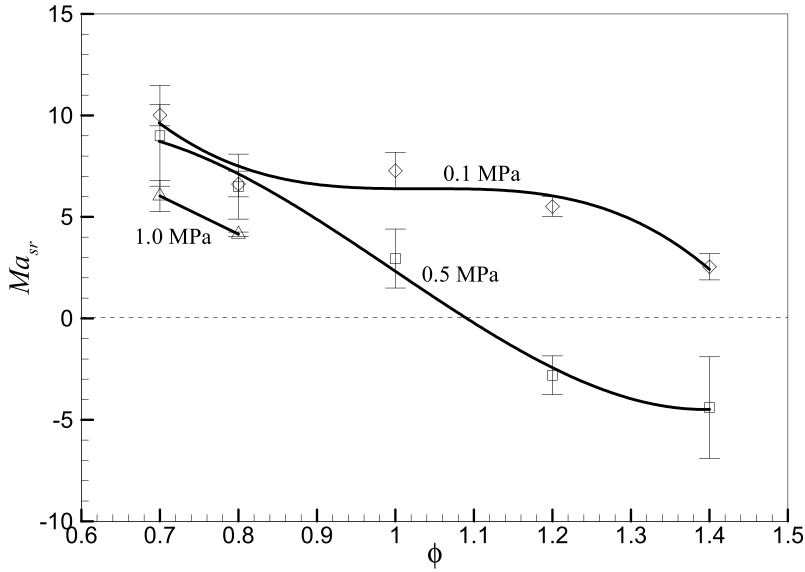


**Figure 8.** Strain rate Markstein number,  $Ma_{sr}$ , of n-butanol/air mixtures at 0.1, 0.5 and 1.0 MPa and 360 K.

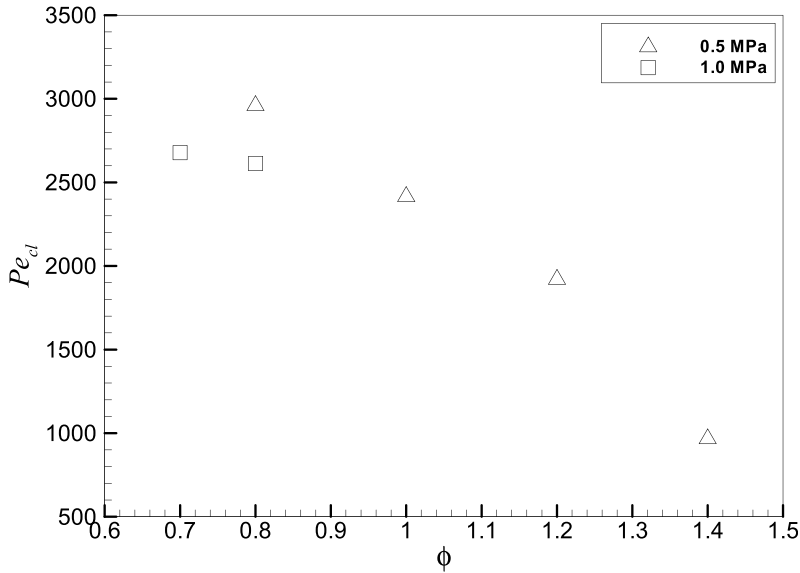


**Figure 9.** Critical peclet number,  $Pe_{cl}$ , of n-butanol/air mixtures against  $\phi$  at 0.5 and 1.0 MPa and 360 K.

Values of Peclet numbers,  $Pe_{cl} = r_{cl}/\delta_l$ , at the onset of cellularity for pressures 0.5 MPa and 1.0 MPa are presented in [Figure 9](#) over a range of  $\phi$  at 360K. Values of  $Pe_{cl}$  decrease with increase in  $\phi$ . An increase in  $\phi$  is associated with higher fuel mass concentrations. The corresponding  $Pe$  decreases with  $\phi$  as thermal diffusivity is predominant that facilitates effective heat dissipation through the flame. This results in hydrodynamic and thermo-diffusive instabilities causing cellular flame

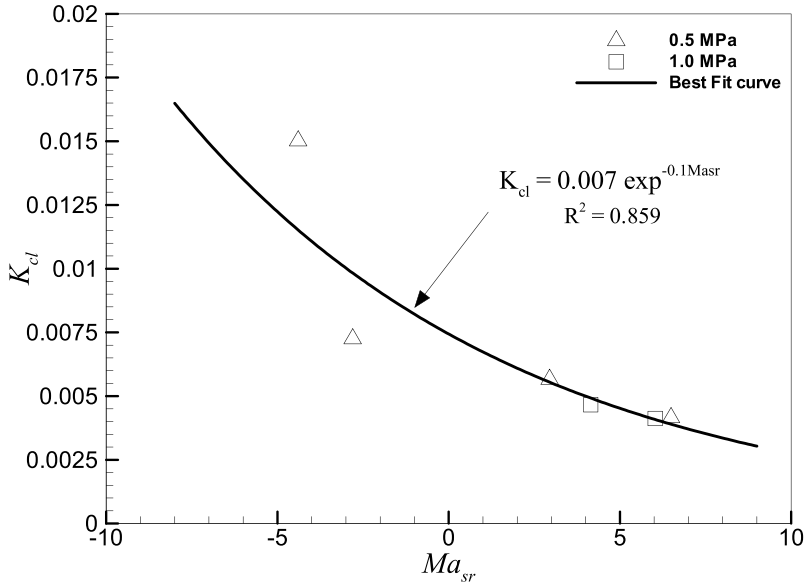


**Figure 10.** Critical Karlovitz stretch factor,  $K_{cl}$ , expressed in terms of  $Ma_{sr}$  for n-butanol/air mixtures; solid line is the best fit curve.

propagation. Consequently, the flame surface area increases leading to rapid flame accelerations. A lower  $Pe$  indicates an early onset of cellularity at smaller flame radii, and therefore, the region of unstable/cellular regime cannot be used to calculate  $u_l$ . In previous studies (Bradley et al. 2007; Gu et al. 2000)  $Pe_{cl}$  are expressed in terms of  $Ma_{sr}$ ; however, it was suggested in (Bradley, Lawes, and Mansour 2009a) that a minimal critical stretch rate, expressed as a critical Karlovitz stretch factor,  $K_{cl}$ , is required for any flame to propagate smoothly below which the flame becomes cellular and is subjected to instability and flame speed accelerations.  $K_{cl}$  is expressed in terms of  $Pe_{cl}$  and  $Ma_b$  as given by the expression (Bradley, Lawes, and Mansour 2009a)

$$K_{cl} = (2/Pe_{cl})(\rho_u/\rho_b)(1 + 2(Ma_b/Pe_{cl}))^{-1} \quad (25)$$

Values of  $K_{cl}$  derived using the above expression for the preset work at 0.5 and 1.0 MPa initial pressures are plotted against their corresponding  $Ma_{sr}$  in Figure 10. Solid line represents the best fit exponential curve. Notwithstanding the uncertainties in  $Ma_{sr}$ , shown by the error bars in Figure 10, a satisfactory correlation (solid line curve) is found with an  $R^2 = 0.859$ . For positive  $Ma_{sr}$ , smaller values of  $K_{cl}$  are sufficient to stabilize the flames. As the  $Ma_{sr}$  values become increasingly negative, higher  $K_{cl}$  values are required to keep the flame stable, narrowing the critical stretch regime which in turn increases the uncertainties in deriving  $Ma_{sr}$  and  $u_l$ . The exponential correlation of  $K_{cl} - Ma_{sr}$  for n-butanol/air mixtures at 360K, shown in Figure 10, closely follows the correlation presented in (Bradley, Lawes, and Mansour 2009a) for ethanol/air mixtures at 358K, suggesting that it is reasonable to present a general correlation of  $K_{cl}$  in terms of  $Ma_{sr}$  independent of fuel and initial experimental conditions.



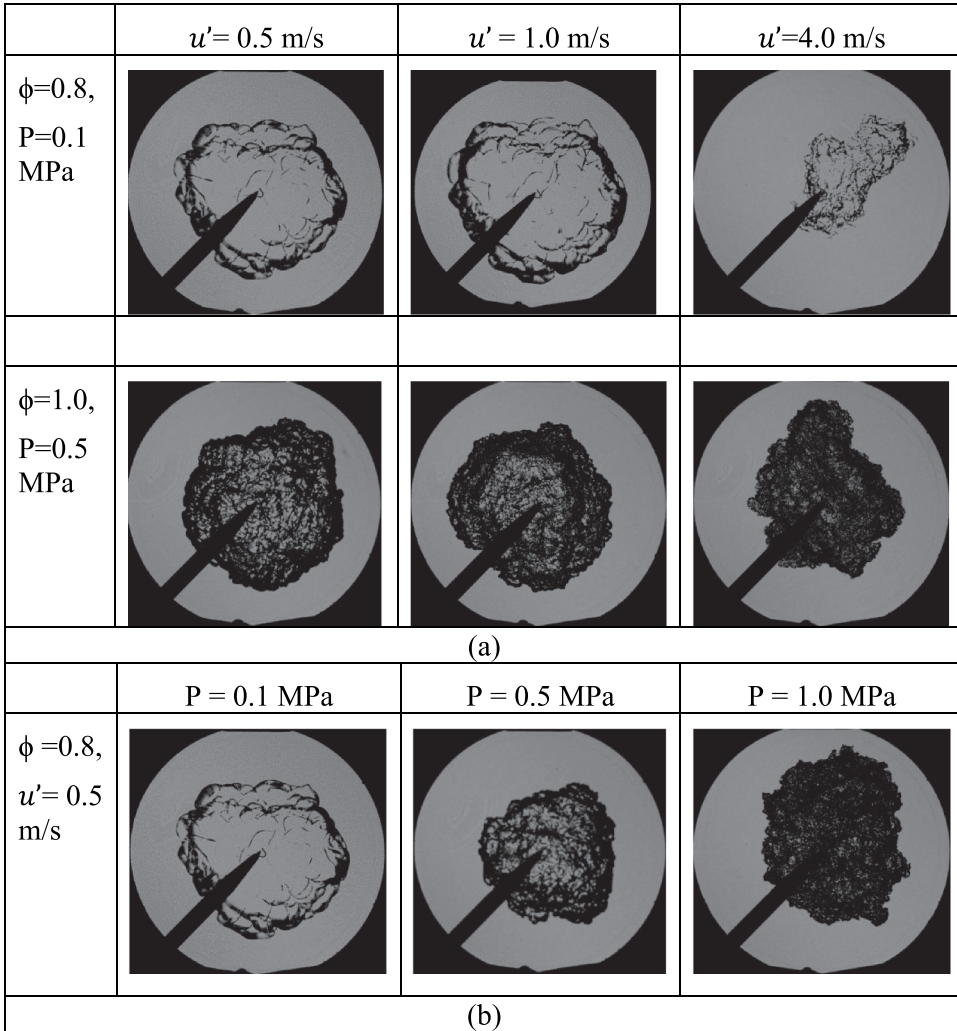


**Figure 11.** Typical turbulent flame images at similar radius (a) at constant initial pressure with increasing  $u'$  (b) at constant  $u'$  and increasing initial pressure.

### **Turbulent burning velocities, $u_{tr}$**

Typical turbulent flame images captured at similar radii are shown in [Figure 11](#). Flames become increasingly wrinkled with  $u'$  and burn with increased flame surface area at higher initial pressures. [Table 2](#) summarizes the range of  $\phi$  and  $u'$  for which the present experiments were conducted. Five identical explosions were conducted at each experimental condition. Mean flame Schlieren radii,  $r_{sch}$ , against time at  $\phi = 1$  for different  $u'$  values at initial temperature and pressure of  $360 \pm 5 \text{ K}$  and  $0.5 \text{ MPa}$ , respectively, are shown in [Figure 12](#). These curves are differentiated to yield the turbulent flame speeds,  $S_{sch} (= \frac{dr_{sch}}{dt})$ , the apparent speed at which the developing flame progresses outwards from the spark.

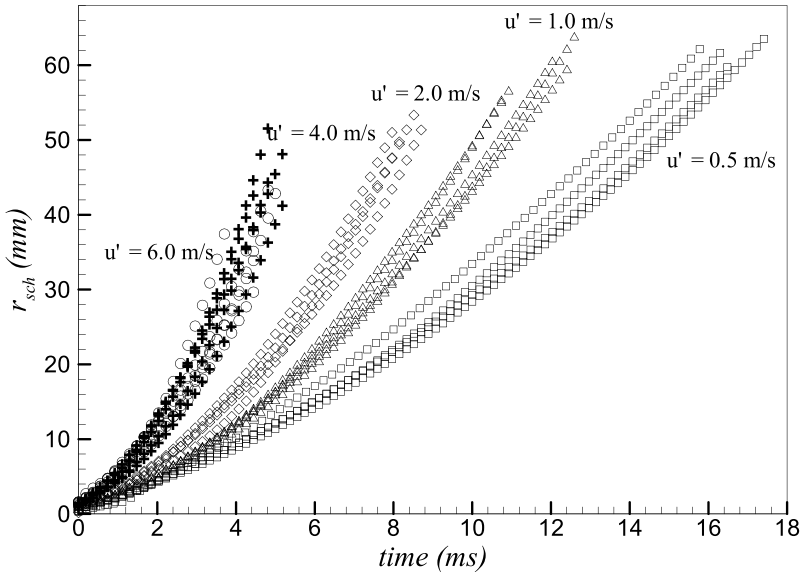


**Figure 12.** Flame radius with increasing time for different  $u'$  at  $\phi = 1$  and 0.5 MPa, 360 K.

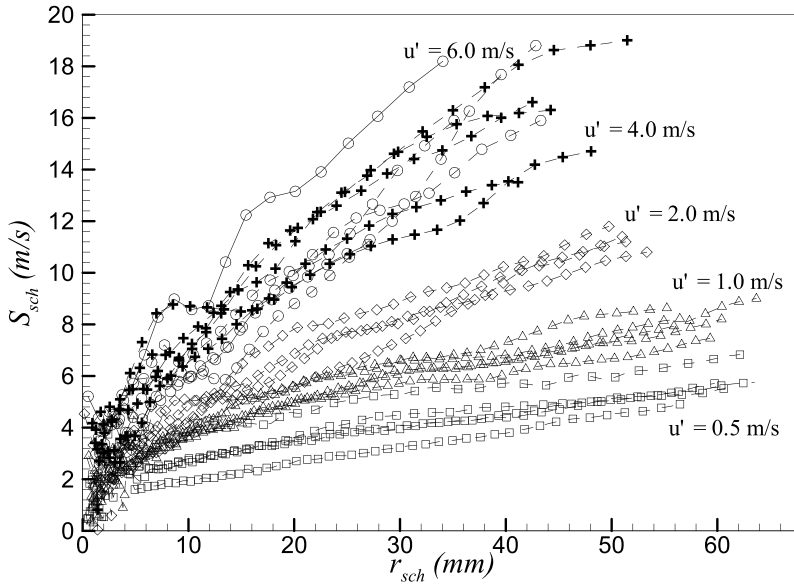


**Figure 13.** Variation of  $S_{sch}$  with increasing radii from ignition for different  $u'$  at  $\phi = 1$  and 0.5 MPa, 360 K.

Shown in **Figure 13** are typical Schlieren flame speeds,  $S_{sch}$ , plotted against Schlieren radii,  $r_{sch}$ , for  $\phi = 1$  and for increasing  $u'$ . The figure demonstrates the inevitable stochastic nature of turbulent burning. At any given value of  $u'$ ,  $S_{sch}$  increased with flame radius  $r_{sch}$  due to the turbulent flame development (Abdel-Gayed, Al-Khishali, and Bradley 1984).  $S_{sch}$  against  $r_{sch}$  for different equivalence ratio,  $\phi$ , and increasing  $u'$  at pressures 0.1 and 0.5 MPa are shown in **Figures 14 and 15** respectively. Each individual curve is the average of five

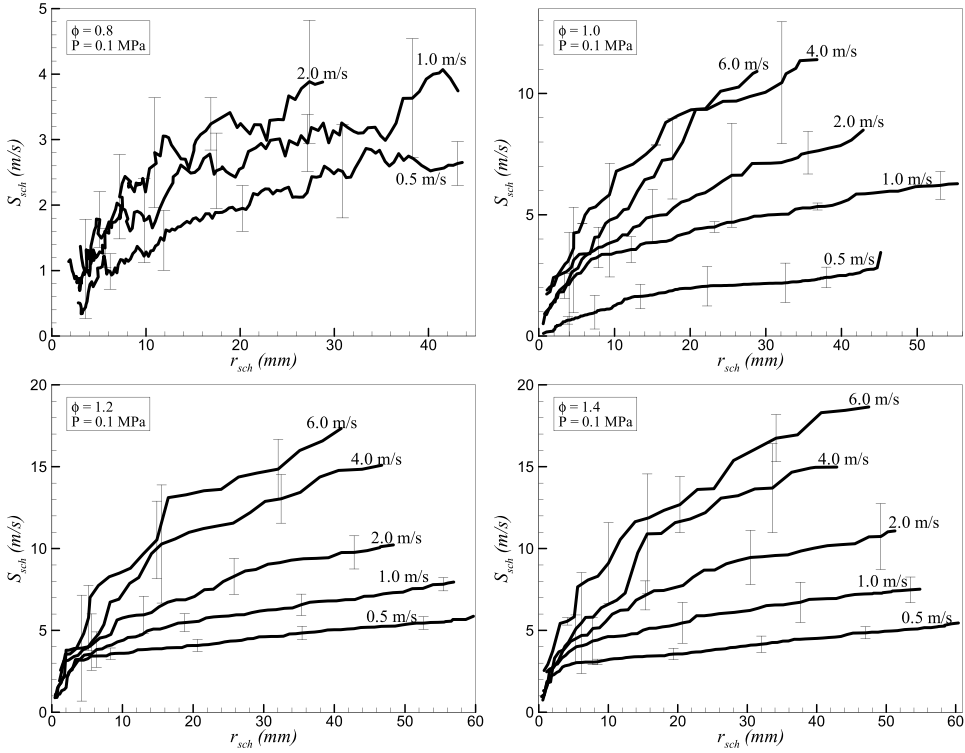


**Figure 14.** Variation of  $S_{sch}$  with increasing radii from ignition for different  $u'$  at  $\phi = 0.8, 1.0, 1.2$  and  $1.4$  at  $0.1$  MPa,  $360$  K.

identical explosions and the error bar denotes the standard deviation. Similar curves at  $1.0$  MPa are presented in Figure A1 in APPENDIX. As discussed before (in Figure 13), for a given  $\phi$  and  $u'$ , each flame has a slightly different  $S_{sch}$  vs  $r_{sch}$  curve due to the instantaneous turbulent flow field, a result of varying turbulent eddies, encountered by the developing flame at different times and at different positions (Lawes et al. 2012). Bradley et al. (1998) found that as the flame grows beyond  $10$  mm radius, it becomes independent of the ignition effect.

It is observed from Figures 14 and 15 that increase in  $\phi$  as well as  $u'$  increases the flame speed. However, at lower values of  $\phi=0.8$  and at low initial pressures of  $0.1$  MPa, the change in  $S_{sch}$  with increasing  $u'$  is less distinguishable due to more scatter in  $S_{sch}$  as the flame develops. This behaviour may be a consequence of the onset of flame quenching. As  $\phi$  is increased, the increase in  $S_{sch}$  is more clear. Highest flame speeds,  $\sim 27$  m/s, are observed at  $\phi = 1.2$  and  $1.4$  and at  $u' = 6.0$  m/s for  $0.5$  MPa. Apparently, at a given radius, no significant change in the flame speeds is observed as  $\phi$  is increased from  $1.2$  to  $1.4$ . However, the scatter is found to be large at higher  $u'$  values irrespective of  $\phi$ , as the flames convect away from the ignition position due to higher turbulence.

Values of  $u_{tr}$  are calculated using Equation 12. For the flame speeds,  $S_{sch}$ , shown in Figures 14 and 15, the corresponding values of  $u_{tr}$  for different  $\phi$  and  $u'$ , are plotted against  $r_{sch}$  in Figures 16 and 17 respectively. Similar curves at  $1.0$  MPa are presented in Figure B1 in APPENDIX. It is suggested in (Lawes et al. 2012) that

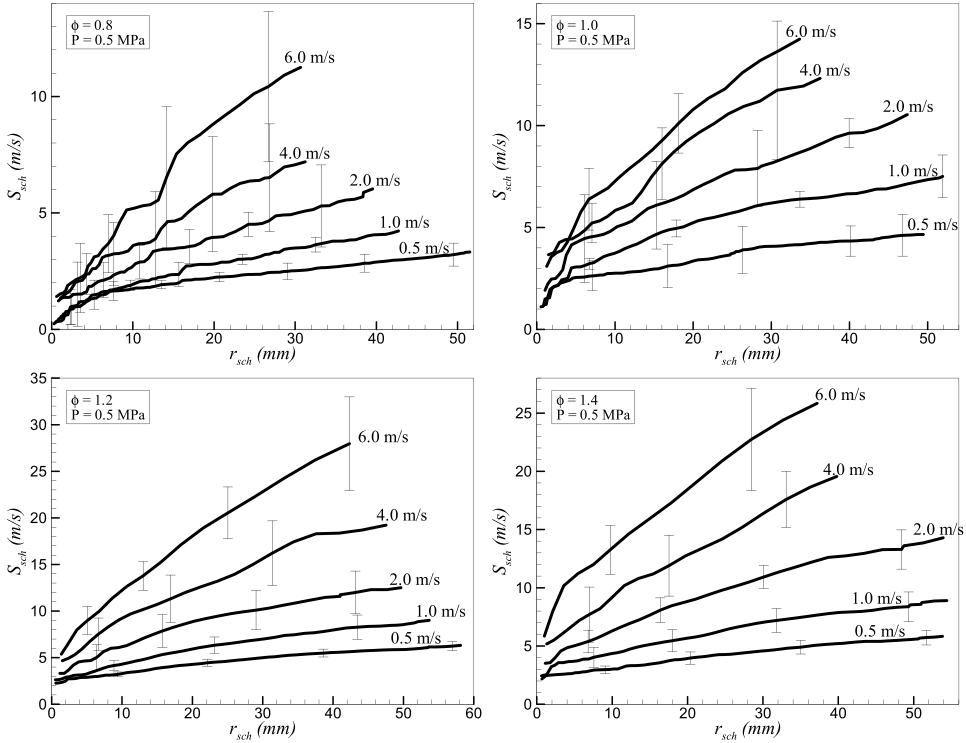


**Figure 15.** Variation of  $S_{sch}$  with increasing radii from ignition for different  $u'$  at  $\phi = 0.8, 1.0, 1.2$  and  $1.4$  at  $0.5$  MPa,  $360$  K.

comparison using flame radius encompasses a wider range of turbulent scales, perhaps it was easier to compare  $u_{tr}$  at a fixed radius. The effect of increasing  $\phi$  and  $u'$  is again found to increase  $u_{tr}$ . Similar to flame speeds, at lower values of  $\phi=0.8$  and at  $0.1$  MPa, the change in  $u_{tr}$  with increasing  $u'$  becomes less distinguishable especially at lower  $\phi$  ( $=0.8$ ) values. Perhaps, it is evident from this plot that  $u_{tr}$  becomes constant with increasing radius at  $u' = 0.5$  m/s. At higher values of  $u' = 1.0$  and  $2.0$  m/s, scatter is increased as the flame grows, which may be a consequence of onset of flame quenching. With the increase in  $\phi$  the change in  $u_{tr}$  is more clear. Maximum values of  $u_{tr}$  are observed at rich mixtures, i.e. at  $\phi = 1.4$  and  $6$  m/s, at  $0.5$  MPa. In contrast to flame speeds,  $u_{tr}$  plots against radius for  $0.1$  and  $0.5$  MPa at  $u' = 2$  and  $4$  m/s reveal noticeable increase in  $u_{tr}$  values at rich mixtures as  $\phi$  is increased from  $1.2$  to  $1.4$ .

Variation of  $u_{tr}$  against increasing  $u'_k$  for different  $\phi$  and  $u'$  at initial pressures varying from  $0.1$  to  $0.5$  MPa are shown in Figures 18 and 19 respectively. Each curve represents the mean from five identical explosions. Similar curves at  $1.0$  MPa are presented in Figure C1 in APPENDIX. Values of  $u_{tr}$  increase with increasing  $u'_k$  and  $u'$ . Maximum values of  $u_{tr}$  are observed for  $u' = 6$  m/s. The effect of increasing  $\phi$  and  $u'$  is again found to increase  $u_{tr}$ . As discussed earlier, the scatter is found to be largest at  $u' = 4$  and  $6$  m/s, irrespective of  $\phi$ . Unlike  $S_{sch}$  vs  $r_{sch}$  and  $u_{tr}$  vs  $r_{sch}$  plots,  $u_{tr}$  vs  $u'_k$  reveals considerable change in  $u_{tr}$  even at low  $\phi$  for different  $u'$ .  $u_{tr}$  values plotted against  $u'_k$  at  $\phi = 0.8$  and at  $0.1$  MPa in Figure 18 show a lot

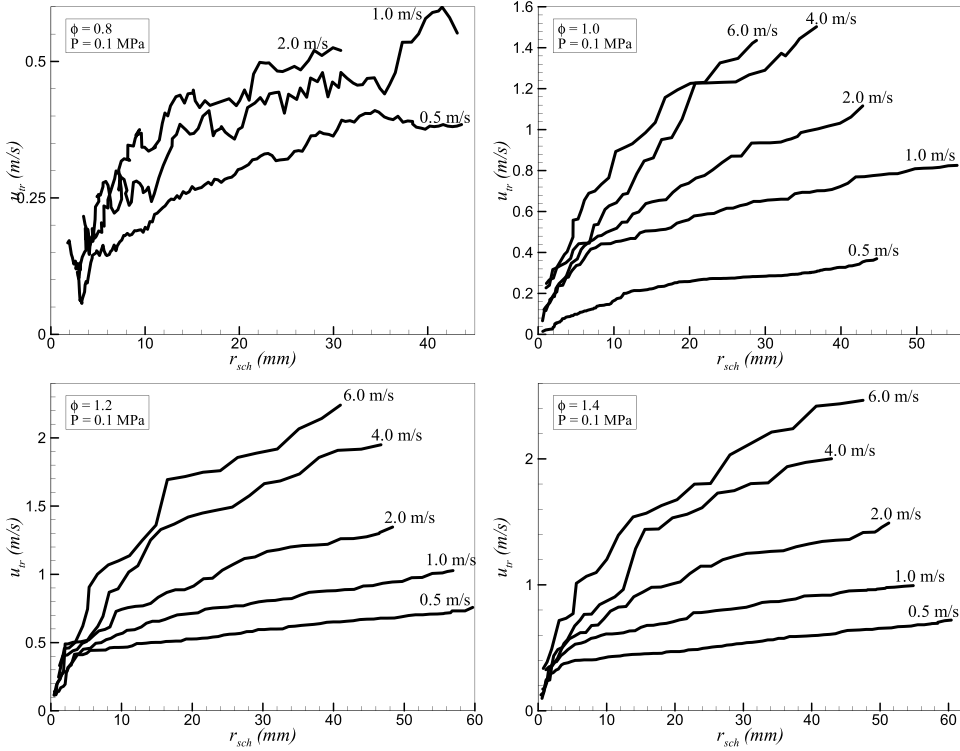


**Figure 16.** Variation of  $u_{tr}$  with increasing radii from ignition for different  $u'$  at  $\phi = 0.8, 1.0, 1.2$  and  $1.4$  at  $0.1$  MPa,  $360$  K.

of variation as the flame is exposed to increasing  $u'_k$ . Further, at  $u' = 2$  m/s,  $u_{tr}$  values cease to increase due to the onset of flame quenching. Pressure affects  $u_{tr}$  significantly when increased from  $0.1$  to  $0.5$  MPa; however, no noticeable change is found with further increase in pressure to  $1.0$  MPa (shown in [Figure C1](#) in APPENDIX).

Shown in [Figures 20–22](#) are  $u_{tr}$ , plotted against  $\phi$  at a flame radius of  $30$  mm at pressures  $0.1, 0.5$  and  $1.0$  MPa respectively. Symbols represent the mean value and the error bars show the standard deviation from five identical explosions. Increased variations in the measurements of  $u_{tr}$  are found at higher  $u'$  and at all pressures. Solid black lines show the best fit curve.  $u_{tr}$  data plotted in [Figure 22](#) for  $\phi = 0.8$  are slightly displaced for better visualisation. The upward arrow in each figure indicates the quench regions where turbulence intensity causes localised flame extinction due to extensive stretching and wrinkling of the flame front with increasing  $u'$ . The values of  $u'_k/u'$  varied between  $0.62$  and  $0.7$  for all  $u'$  at  $0.1, 0.5$  and  $1.0$  MPa (Lawes et al. 2012). The flames developed at this radius experienced  $62$ – $70\%$  of the turbulent spectrum with no spark influence, indicating the measurements and comparisons made at this radius are quantifiable. Generally observing,  $u_{tr}$  gradually increased from  $\phi = 0.8$  to  $\phi = 1.0$ . For flames at  $u' = 0.5$  m/s, the maximum value of  $u_{tr}$  occurred at  $\phi = 1.2$  and tends to decrease beyond this limit. At  $u' = 1.0$  m/s, values of  $u_{tr}$  at  $\phi = 1.4$  reached similar to  $\phi = 1.2$ . However, at  $u' = 2.0, 4.0$  and  $6.0$  m/s, richest mixture at  $\phi = 1.4$  burned noticeably faster than at other  $\phi$  values. Larger scatter in the  $u_{tr}$  values are observed at  $u' = 6.0$  m/s irrespective of  $\phi$  and pressure. Flames quenched at  $u' = 4$  m/s for  $\phi = 0.8$  at  $0.1$  MPa

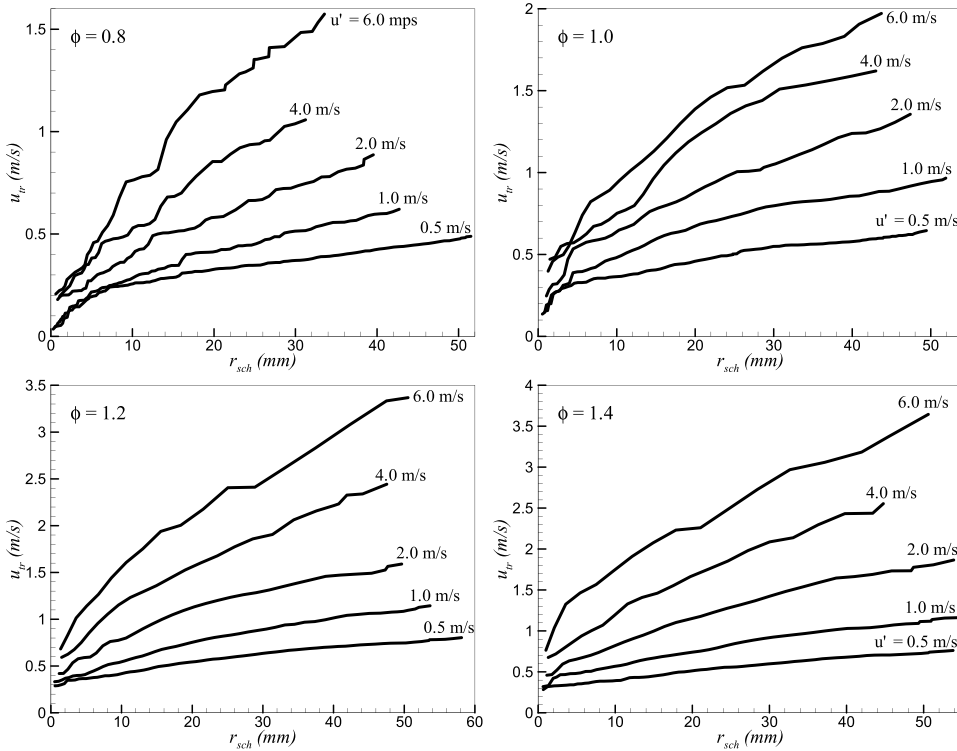


**Figure 17.** Variation of  $u_{tr}$  with increasing radii from ignition for different  $u'$  at  $\phi = 0.8, 1.0, 1.2$  and  $1.4$  at  $0.5$  MPa,  $360$  K.

while at  $0.5$  and  $1.0$  MPa complete flame propagation was observed. Further lower equivalence ratios, i.e.  $\phi = 0.7$ , resulted in flame quenching at lower  $u'$  at all initial pressures. At higher pressures,  $0.5$  MPa and  $1.0$  MPa, and at leaner mixtures,  $\phi = 0.7$ , complete flame quenching was observed at lower values of  $u' = 2\text{ m/s}$  and  $u' = 1\text{ m/s}$  respectively. On the other hand, at  $0.1$  MPa initial pressures and at  $\phi = 0.7$ , 80% flame propagation, indicated by  $P_b = 0.8$  in Figure 20, was observed at  $u' = 1\text{ m/s}$ . Further increase in  $u'$ , up to  $2\text{ m/s}$ , resulted in 20% flame propagation ( $P_b = 0.2$ ). Due to high  $Ma_{sr}$  values at low  $\phi$ , even lower levels of turbulence is sufficient for the flames to quench. As turbulence further increases, the entire flame extinguishes, leading to global quench preventing further combustion. Identifying quench regions is key for accurately predicting flame behaviour, combustion efficiency and emissions that would aid in designing efficient combustion systems and predict explosion hazards.

$u_{tr}$ , for n-butanol/air mixtures, obtained in the present work are compared with the  $u_{tr}$  for iso-octane/air mixtures reported in (Lawes et al. 2005, 2012) at the same conditions,  $0.5$  MPa and  $360\text{ K}$  at different  $u'$ , in Figure 23. Both experiments were carried out in the same Leeds combustion vessel. Experimental values of  $u_{tr}$ , at a flame radius of  $30\text{ mm}$ , are plotted against  $\phi$  for different  $u'$  for both fuels. It is interesting to note that the trends are similar, however, at same temperature and pressure and for a given  $u'$ , n-butanol/air mixtures yielded higher  $u_{tr}$  compared to iso-octane/air mixtures. These results are in line with the results presented in (Aleiferis, Serras-Pereira, and Richardson 2013; Serras-Pereira,

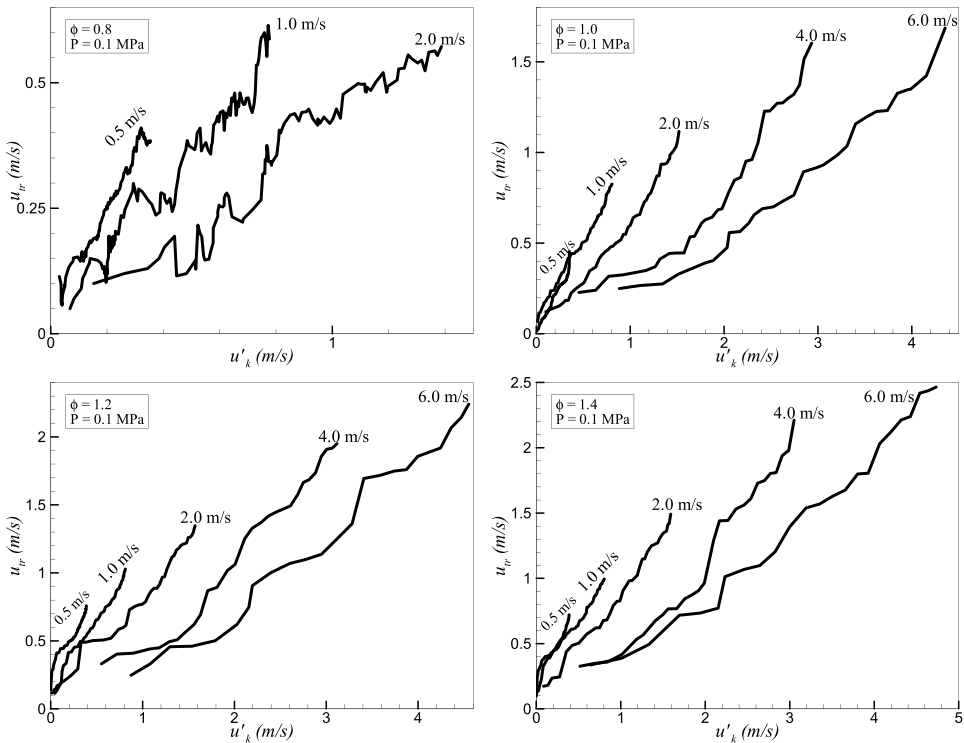


**Figure 18.** Variation of  $u_{tr}$  with  $u'_k$  for different  $u'$  at  $\phi = 0.8, 1.0, 1.2, 1.4$  at 0.1 MPa, 360 K.

Aleiferis, and Richardson 2013), comparing iso-octane and n-butanol as a fuel in spark ignition engines. The higher  $u_{tr}$  values obtained for n-butanol/air mixtures can be attributed to the lower  $Ma_{sr}$ , shown in Figure 24, compared to iso-octane/air mixtures. It has been shown (Bradley, Gaskell, and Gu 1998) that under turbulent conditions positive  $Ma_{sr}$  decreases the burning velocity, while mixtures with negative  $Ma_{sr}$  tend to burn faster.  $u_{tr}$  increased with  $\phi$  as well as  $u'$ . It is interesting to note that the rate of increase in  $u_{tr}$  for n-butanol/air mixtures are found to be higher than iso-octane/air mixtures at higher  $u'$ . Iso-octane flames quenched at  $u' = 4 \text{ m/s}$  and  $\phi = 0.8$ . On the other hand, for the same  $\phi$  value n-butanol flames burned efficiently even at  $u' = 6 \text{ m/s}$ .

## Discussion

Results of  $u_l$ ,  $L_b$  and  $Ma_{sr}$  along with the corresponding mixture properties are presented in Table 4. Lowest values of  $u_l$  are observed for lean mixtures at  $\phi = 0.8$ .  $u_l$  increased with  $\phi$ . Highest values of  $u_l$  are obtained for slightly rich mixtures,  $\phi = 1.1$ . Further increase in  $\phi$  decreased  $u_l$ . Although the values of  $L_b$  and  $Ma_{sr}$ , in Table 3, for the same set of conditions are repeatable,  $Ma_{sr}$  varies over a larger value at  $\phi = 1.4$ .  $Ma_{sr}$  decreased with increase in  $\phi$ . Highest values of  $Ma_{sr}$  are obtained for lean mixtures while rich mixtures resulted in lower  $Ma_{sr}$ . For very rich mixtures,  $\phi = 1.4$ , it was not possible to determine  $L_b$  and  $Ma_{sr}$  due to the onset of cellularity at an early stage from ignition.

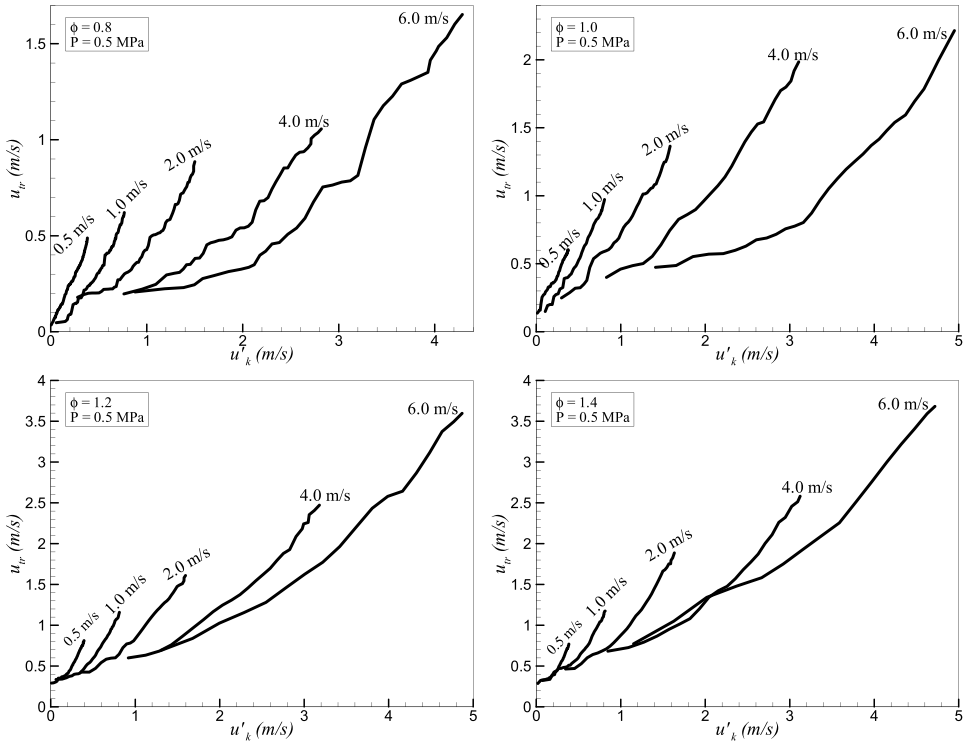


**Figure 19.** Variation of  $u_{tr}$  with  $u'_k$  for different  $u'$  at  $\phi = 0.8, 1.0, 1.2$  and  $1.4$  at  $0.5$  MPa,  $360$  K.

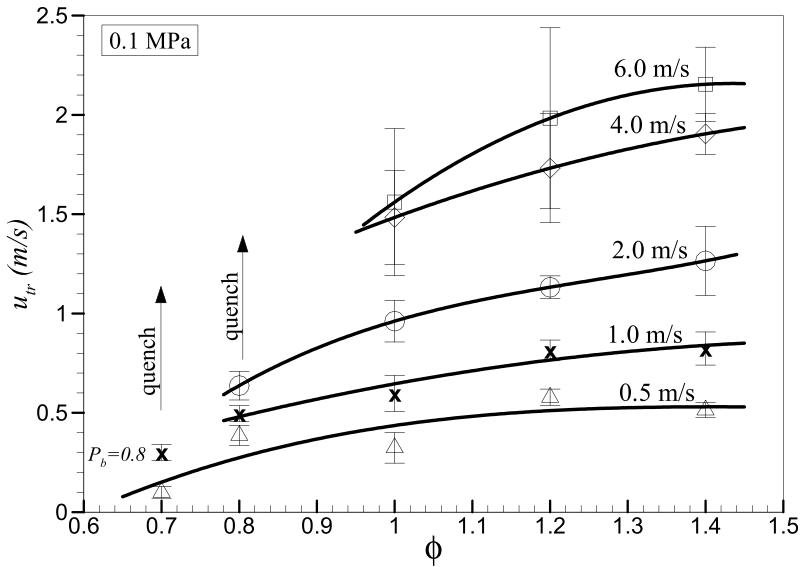


**Figure 20.**  $u_{tr}$ , for n-butanol/air at  $r_{sch} = 30$  mm against  $\phi$  for different  $u'$  at  $0.1$  MPa,  $360$  K; solid line shows the best fit curve for the experimental data.



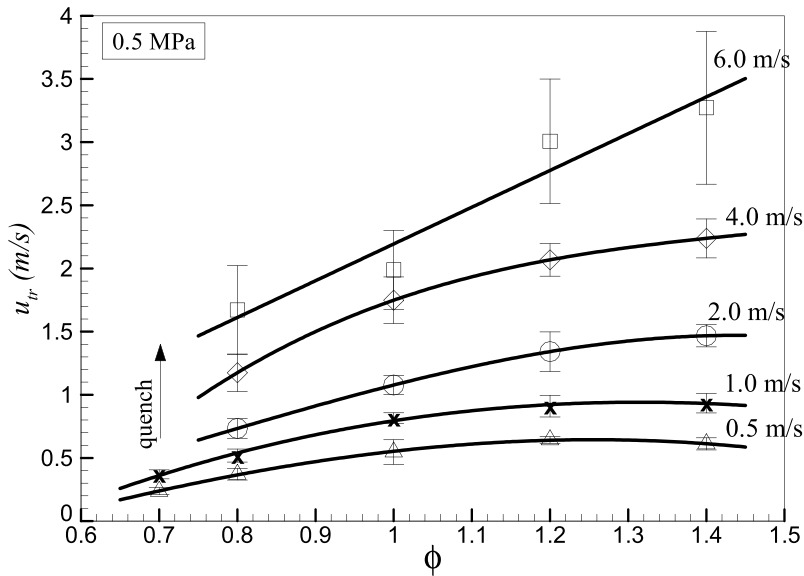


**Figure 21.**  $u_{tr}$ , for n-butanol/air at  $r_{sch}=30\text{mm}$  against  $\phi$  for different  $u'$  at 0.5 MPa, 360 K; solid line shows the best fit curve for the experimental data.

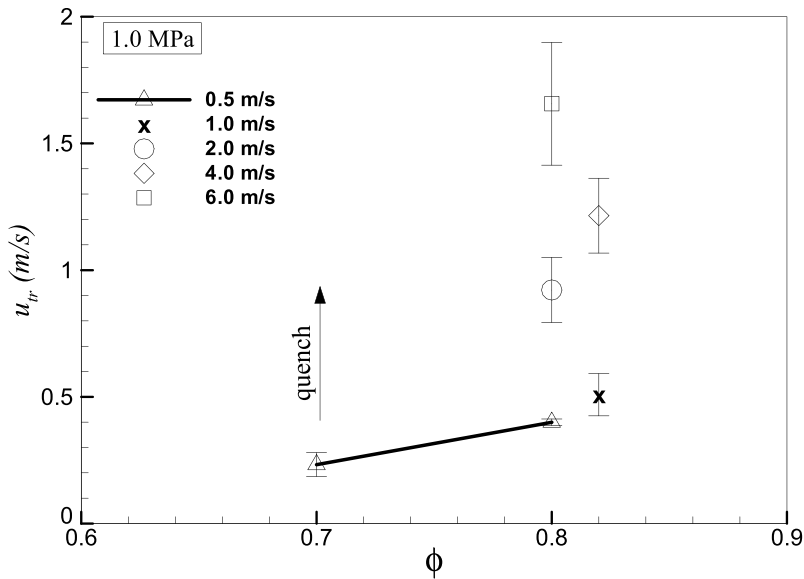


**Figure 22.**  $u_{tr}$ , for n-butanol/air at  $r_{sch}=30\text{mm}$  against  $\phi$  for different  $u'$  at 1.0 MPa, 360 K; solid line shows the best fit curve for the experimental data.

Compared in Figure 25 is the ratio  $u_{tr}/u_l$  against  $\phi$ , compared at a flame radius of 30 mm, for n-butanol and iso-octane flames at 0.5 MPa and 360K. Magnitude of  $u_{tr}$  is approximately 3.2 times higher than  $u_l$  for n-butanol flames from  $\phi=0.8$  to 1.2 and increases to 5 with further increase in  $\phi$ . Lean iso-octane flames are seen to exhibit the

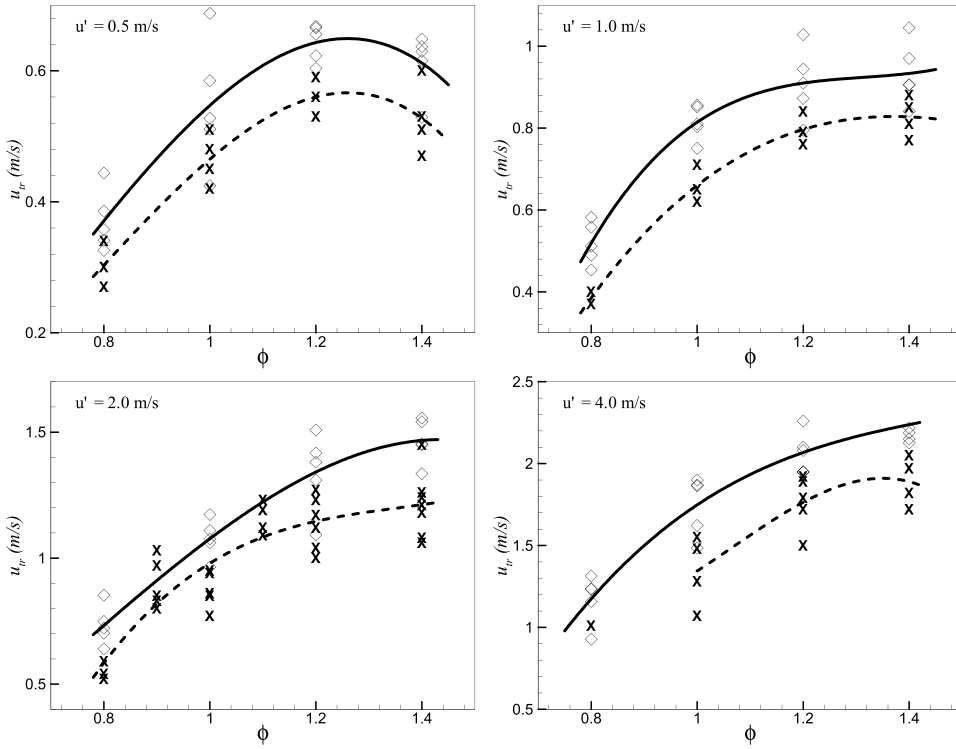


**Figure 23.** Comparison of  $u_{tr}$ , for n-butanol/air (open diamonds) and iso-octane/air (crosses) at  $r_{sch}=30\text{mm}$  against  $\phi$  for different  $u'$  at 0.5 MPa, 360 K; solid curve shows the best fit for present n-butanol experimental data, dashed curve show the best fit for iso-octane/air data (Lawes et al. 2012).

lowest  $u_{tr}/u_l$  at  $\phi = 0.8$ ; however, it increases steadily with  $\phi$  till  $\phi = 1.4$ . Values of  $u_{tr}/u_l$  are relatively higher for n-butanol/air mixtures compared to iso-octane over the range of  $\phi = 0.8$  to 1.2. However, both exhibit a similar trend beyond this value. The behaviour of higher values of  $u_{tr}/u_l$  for n-butanol corroborates with the results of  $Ma_{sr}$ , as shown in Figure 24. The lower  $Ma_{sr}$  values of n-butanol would well justify the higher  $u_{tr}/u_l$  ratio from  $\phi = 0.8$  to 1.2. Although the measurements of  $Ma_{sr}$ , at  $\phi = 1.4$  for iso-octane were not reported in (Lawes et al. 2005, 2012) due to the flames becoming cellular from inception, it can be predicted from the behaviour of  $u_{tr}/u_l$  that  $Ma_{sr}$  values would be similar for both iso-octane and n-butanol. Quenching was not observed for n-butanol flames at any of the conditions between the limits compared, indicating appreciable burning rates over a wide range of  $\phi$  employed.

The obtained experimental data of  $u_{tr}$  for n-butanol/air mixtures are correlated in terms of  $u_{tr}/u'_k$  and  $K$ , at flame radius of 30 mm. Moreover, it is suggested that the influence of  $Ma_{sr}$ , due to flame straining, over curvature,  $Ma_c$ , is dominant in increasing turbulent burning velocities (Bradley et al. 2003). Therefore, the correlation  $u_{tr}/u'_k$  against  $K$  is presented in terms of  $Ma_{sr}$ , and that due to curvature may be neglected at this stage. Values of  $u_l$ ,  $v$ ,  $Ma_{sr}$  used for these correlations are given in Table 4.  $Ma_{sr}$  values were quite repeatable for lean and stoichiometric mixtures, while at higher  $\phi$  values the variation was large, especially at higher pressures. Values of  $u_{tr}/u'_k$  are presented for both positive and

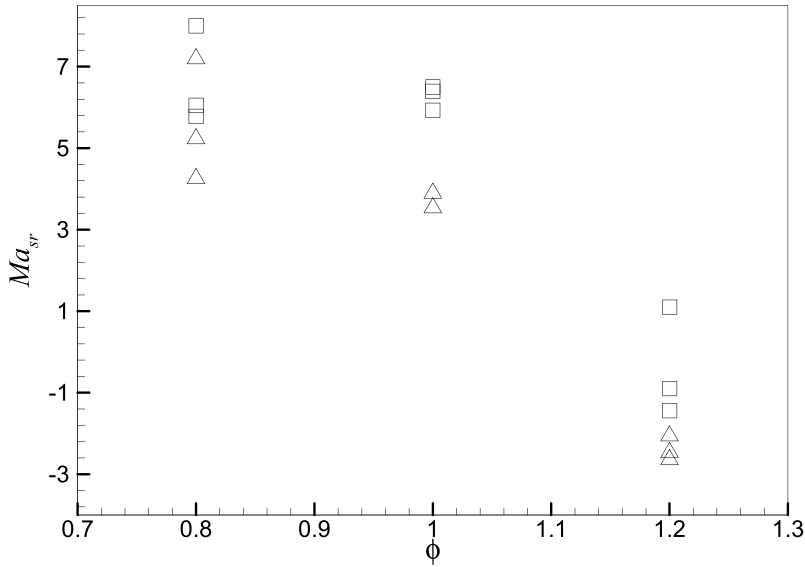


**Figure 24.** Strain rate Markstein numbers,  $Ma_{sr}$  of n-butanol (open triangles) and iso-octane/air (open squares, (Lawes et al. 2005, 2012)) flames against  $\phi$  at 0.5 MPa and 360 K.

**Table 4.** Laminar flame properties at 0.1, 0.5, 1.0 MPa and 360 K.

$\phi$	0.1 MPa					0.5 MPa					1.0 MPa				
	$\rho_u/\rho_b$	$vx10^{-5}$	$u_l$	$L_b$	$Ma_{sr}$	$\rho_u/\rho_b$	$vx10^{-6}$	$u_l$	$L_b$	$Ma_{sr}$	$\rho_u/\rho_b$	$vx10^{-6}$	$u_l$	$L_b$	$Ma_{sr}$
0.7	5.61	2.14	0.29	2.40	10.01	5.62	4.27	0.14	0.80	9.00	5.62	2.14	0.11	0.41	6.03
0.8	6.11	2.13	0.33	1.68	6.62	6.13	4.25	0.21	0.60	6.49	6.14	2.13	0.17	0.12	4.15
1.0	6.85	2.11	0.45	1.45	7.27	6.95	4.21	0.31	0.28	2.95	—	—	—	—	—
1.2	6.97	2.09	0.53	1.05	5.51	6.99	4.17	0.36	0.10	-2.80	—	—	—	—	—
1.4	6.81	2.07	0.42	0.25	2.54	6.82	4.14	0.29	-0.43	-4.39	—	—	—	—	—

negative values of  $Ma_{sr}$  in Figure 26. The open symbols in the graph represent the average experimental values of  $u_{tr}/u'_k$  for five explosions at different  $Ma_{sr}$ . Solid lines represent the best fit curves. For a given  $Ma_{sr}$ ,  $u_{tr}/u'_k$  has higher values at lower  $K$  and reduces with increase in  $K$ . For a given  $K$ , at negative  $Ma_{sr}$ ,  $u_{tr}/u'_k$  values are the highest and decrease as  $Ma_{sr}$  becomes positive.

The present measurements of  $u_{tr}/u'_k$  are compared with the  $u_{tm}/u'_k$  values obtained from the correlation of (Bradley, Lawes, and Mansour 2011) for different strain rate Markstein numbers,  $Ma_{sr}$ . The expression used to obtain  $u_{tm}/u'_k$  correlation in terms of  $K$  is given by

$$U = u_{tm}/u'_k = A_m \alpha K^\beta \text{ for } K \geq 0.05 \quad (26)$$

Here  $A_m = 1$ ,  $\alpha$  and  $\beta$  are constants given by the equations in terms of  $Ma_{sr}$  as

$$\alpha = \begin{cases} 0.023(30 - Ma_{sr}), & \text{if } Ma_{sr} \text{ is } +ve \\ -0.085(7 - Ma_{sr}), & \text{if } Ma_{sr} \text{ is } -ve \end{cases}$$

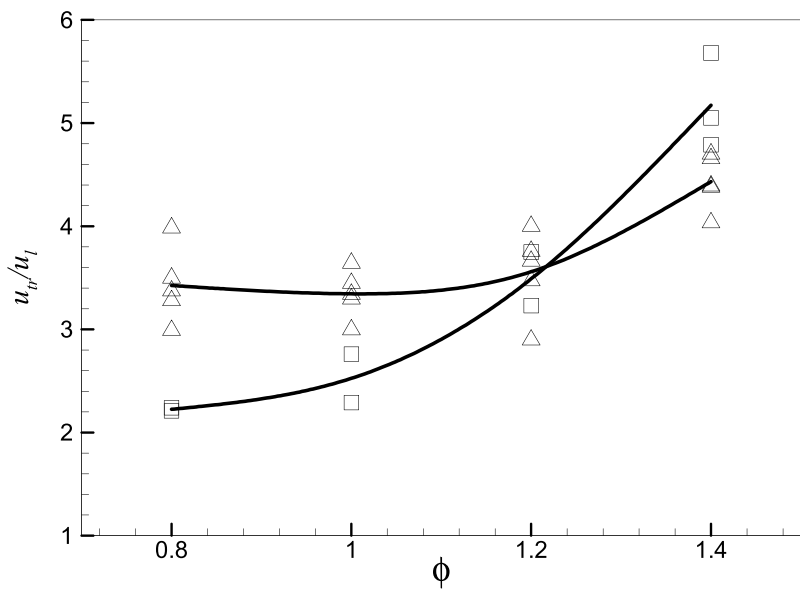


**Figure 25.**  $u_{tr}/u_l$  of n-butanol (open triangles) and iso-octane/air (open squares, (Lawes et al. 2005, 2012)) flames against  $\phi$  at 0.5 MPa and 360 K.

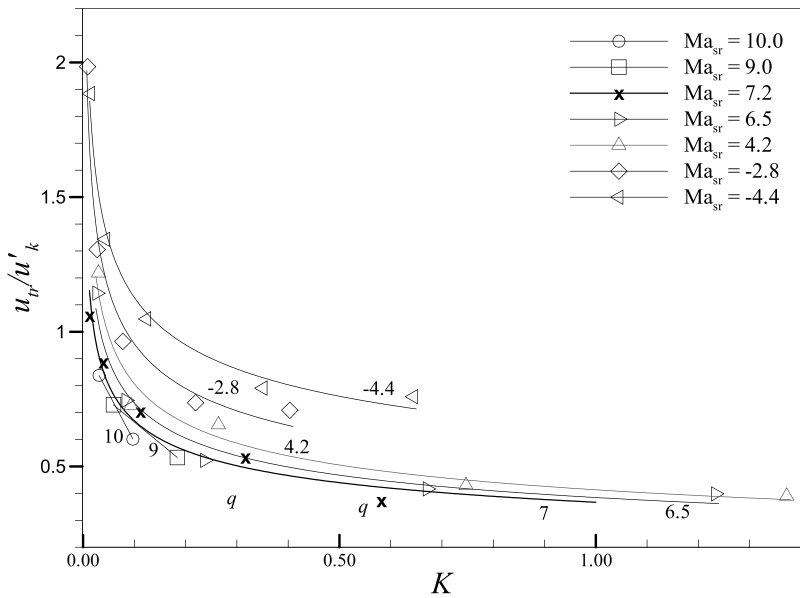


**Figure 26.** Correlation of  $u_{tr}/u'_k$  with  $K$  using Schlieren experiments.

$$\beta = \begin{cases} 0.0103(Ma_{sr} - 30), & \text{if } Ma_{sr} \text{ is } +ve \\ -0.0075(30 + Ma_{sr}), & \text{if } Ma_{sr} \text{ is } -ve \end{cases}$$

Here  $u_{tm}$  is the turbulent burning velocity associated with pressure rise measured using a pressure transducer during an explosion. The details of measuring  $u_{tm}$  are presented in (Bradley, Lawes, and Mansour 2011). In order to compare the correlated experimental data of  $u_{tr}/u'_k$  presented in Figure 26 with that of equation (24), it was necessary to convert this data in terms of  $u_{tm}/u'_k$ . This was achieved by using the relation between  $u_{tm}$  and  $u_{tv}$  given in (Bradley, Lawes, and Mansour 2011)

$$u_{tm}/u_{tv} = (r_v/r_m)^2 \quad (27)$$

Here  $r_v$  and  $r_m$  are the radius associated with flame surfaces obtained from Mie scattered images and pressure transducer records respectively (Bradley, Lawes, and Mansour 2011). In the present study,  $u_{tv}$ , associated with  $r_v$ , is obtained using Equation 12. The ratio of  $r_v/r_m$  in Equation 27 is again obtained from (Bradley, Lawes, and Mansour 2011). Shown in Figure 27 are the correlated  $u_{tm}/u'_k$  curves, obtained in the present experimental

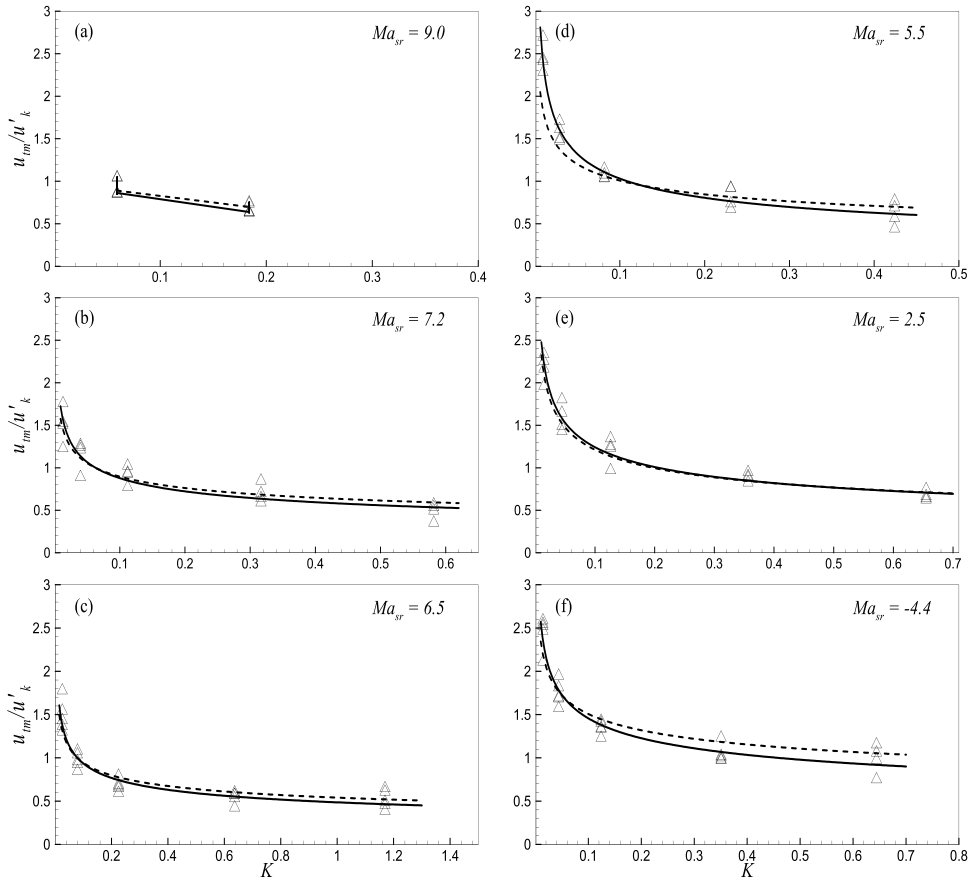


**Figure 27.** Correlation of  $u_{tm}/u'_k$  with  $K$  using Schlieren experiments (open triangles); and broken curve using the equation (24); solid curve shows the best fit for data from present Schlieren experiments.

measurements, compared with those calculated using equation (24), for different  $Ma_{sr}$ . The open triangles represent the experimental data from five different explosions. The solid curve shows the best fit, whereas, the broken curve represent  $u_{tm}/u'_k$  values obtained using equation (24). The coefficient of determination,  $R^2$ , ranged between 0.85 and 0.92 for the experimental data shown in Figure 27. Generally both the curves decrease with increasing  $K$  for a given  $Ma_{sr}$ . For  $K < 0.1$ , a sudden increase in both  $u_{tm}/u'_k$  values were observed. Notwithstanding the inevitable scatter during turbulent burning velocity measurements, it is striking that both the curves agree quite satisfactorily except for values of negative  $Ma_{sr}$ , shown in Figure 8, are subjected to increased scatter. It is interesting to note that the experimental values of  $u_{tm}/u'_k$  are generally higher than the ones obtained using equation (24) for the region  $K < 0.03$  in particular for lower  $Ma_{sr}$  indicating that the correlation given by equation (24) holds good for  $K \geq 0.05$ . For very positive values of  $Ma_{sr}$  there is a good agreement between the two curves. It was suggested (Bradley et al. 2005, 2007) that flames in the lower  $K$  region,  $K \leq 0.05$ , are subjected to thermoacoustic instabilities that enhance burning velocities a consequence of high flame stretch rate. The calculations of  $u_{tm}/u'_k$  in Figure 27 corroborates this argument. A consequence of an increase in  $K$  results in increased merging of flamelets and localised flame extinctions that contribute to the gradual decrease in  $u_{tm}/u'_k$  (Bradley et al. 2005).

The correlated curves of Figure 27 are reproduced on Figures 28 and 29 for both positive and negative  $Ma_{sr}$  values respectively. Also shown in these figures are the experimentally deduced values of  $u_{tm}/u'_k$  against  $Ma_{sr}$  from past work (Bradley et al. 2013; Bradley, Lawes, and Mansour 2011, 2011; Kitagawa et al. 2008; Mandilas et al. 2007; Shepherd and Cheng 2001). Each curve is represented by an  $Ma_{sr}$  value followed by a reference number from

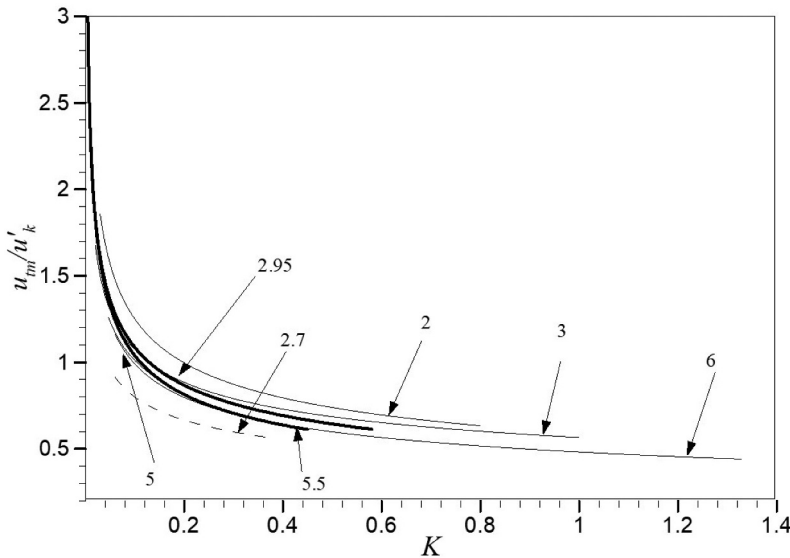


**Figure 28.**  $u_{tm}/u'_k$  plotted against  $K$  for positive  $Ma_{sr}$ . Thick solid lines ( $Ma_{sr} = 2.95$  and  $5.5$ ) are the present work. Thin solid lines ( $Ma_{sr} = 2$  and  $6$  (Mandilas et al. 2007),  $Ma_{sr} = 2.7$  (Shepherd and Cheng 2001),  $Ma_{sr} = 3$  and  $5$  (Bradley et al. 2013; Bradley, Lawes, and Mansour 2011, 2011) represent the work from previous studies.

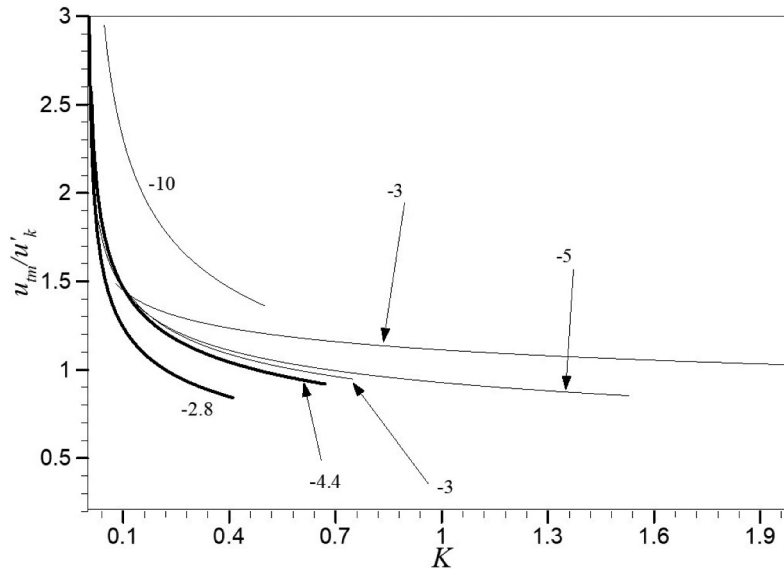


**Figure 29.**  $u_{tm}/u'_k$  plotted against  $K$  for negative  $Ma_{sr}$ . Thick solid lines ( $Ma_{sr} = -2.8$  and  $-4.4$ ) are the present work. Thin solid lines ( $Ma_{sr} = -3$  (Bradley, Lawes, and Mansour 2011, 2011; Mandilas et al. 2007)),  $Ma_{sr} = -5$  (Bradley et al. 2013) and  $Ma_{sr} = -10$  (Kitagawa et al. 2008)) represent the work from previous studies.

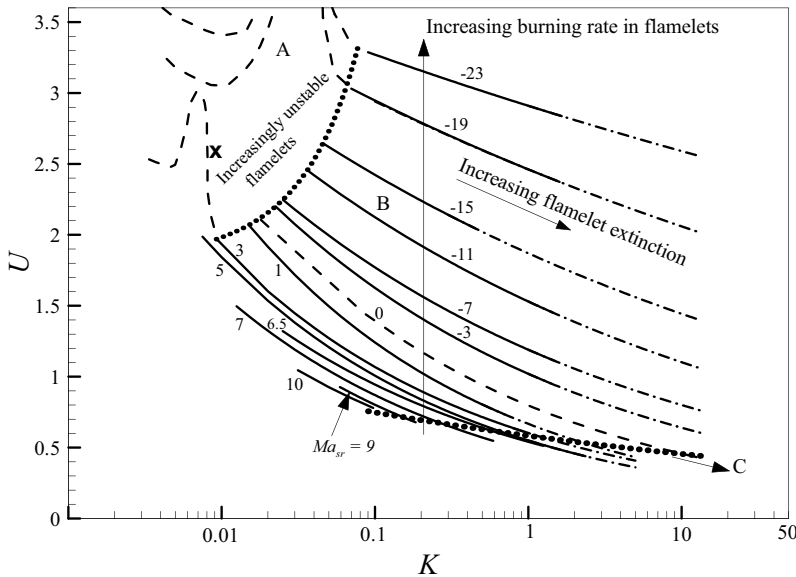


**Figure 30.** Regimes of turbulent combustion shown in terms of  $u_{tm}/u'_k$  against  $K$  over a range of  $Ma_{sr}$ .

where it was taken. Solid thick curves shown are the present work with an  $Ma_{sr}$  not followed by any reference number. The agreement among the correlations from different work, which include different fuels and different values of  $\phi$ , is quite satisfactory among the

combustion vessel data except for the burner data, represented by the broken curve in Figure 28. However, the curves at negative  $Ma_{sr}$ , shown in Figure 29, exhibit a noticeable discrepancy that can be attributed to the different methods adopted to derive  $Ma_{sr}$ . Nonetheless, the curves, for both positive and negative  $Ma_{sr}$  are in good agreement with the past combustion data obtained in the present Leeds combustion vessel, indicating that the proposed correlation, given by equation (24), holds well for the current results.

Shown in Figure 30 are the  $u_{tm}/u'_k$  vs  $K$  curves for different  $Ma_{sr}$ . The figure presents different turbulent combustion regimes which are detailed in (Bagdanavicius et al. 2015; Bradley et al. 2013). Shown in this figure is the work reproduced from (Bradley et al. 2013) as well as the present data extending the  $u_{tm}/u'_k$  values from  $Ma_{sr} = 5$  to more positive  $Ma_{sr} = 10$ . In general  $u_{tm}/u'_k$  curves decrease with  $K$  while it for a given  $K$  value it increases with a decrease in  $Ma_{sr}$ . The figure shows three different turbulent combustion regimes denoted by A, B and C. Regime A features the lower  $K$  region with higher  $U$  values. Interestingly, this region denotes an increasingly unstable flamelet region where the interactions with thermoacoustic instabilities play a predominant role in enhancing the  $U$  values. This region is currently being explored at University of Leeds to gain more insights between the interactions of different mechanisms at play. Regime B represents a stable region where flames are wrinkled proportionally with turbulent that in turn increases the turbulent burning. Increasing the  $K$  value further causes increased flamelet extinction and ultimate flame quenching and this region is indicated by Regime C. The present study contributes to the latter two regimes i.e. Regime B and Regime C. The broken curve at the bottom right indicates the onset of flame extinctions with 80% probability of burning,  $P_{b0.8}$ . With increase in  $Ma_{sr}$  values lower levels of turbulence is sufficient for the flames to quench. The broken curve of flame quenching has been extended further through the more positive  $Ma_{sr}$  curves of Regime B. It is interesting to see the behaviour of  $u_{tm}/u'_k$  against  $K$  holds true for the extended positive  $Ma_{sr}$  values, i.e. an increase in  $Ma_{sr}$  decreases the  $u_{tm}/u'_k$  over increasing values of  $K$ . Unlike the previous quench regime identified in (Bagdanavicius et al. 2015; Bradley et al. 2013), the quench curve at higher  $K$  values is corrected as flames could still be seen propagating beyond  $Ma_{sr} = -3$ .

## Conclusions

Fundamental studies of  $u_l$ , and  $u_{tr}$ , of premixed n-butanol/air mixtures are carried out using spherically expanding flames in a constant volume chamber. The main results are summarised as follows:

- (1)  $u_l$ , and the associated  $L_b$ ,  $Ma_{sr}$ ,  $Pe_{cl}$  and the corresponding  $K_{cl}$  associated with the onset of flame instabilities are presented.
- (2)  $u_l$  reduced with increasing pressure. Minimum values of  $u_l$  are observed for lean mixtures, i.e. at  $\phi = 0.7$ .  $u_l$  increased with  $\phi$ . The peak values of  $u_l$  for a given pressure are observed to be on the richer mixture side, i.e. at  $\phi = 1.1$ .
- (3)  $L_b$  decreases with increasing pressure and  $\phi$ . At 0.5 MPa,  $L_b$  reached negative values at rich mixtures, resulting in an increase in burning rate with stretch.
- (4)  $Ma_{sr}$  decreases with pressure and increasing  $\phi$ , with values becoming eventually negative at high pressures and rich mixtures.



- (5) For the data measured in the present study, a satisfactory correlation exists between  $K_{cl}$ , and  $Ma_{sr}$  with an  $R^2$  value of 0.859. It is currently understood that it is more rational to express instabilities in terms of  $K_{cl}$  rather than  $Pe_{cl}$  alone.
- (6) Turbulent burning rates of n-butanol/air mixtures at high initial temperatures and up to 1.0 MPa in a controlled environment are reported for the first time.  $u_{tr}$ , values increase with increase in both  $\phi$  and  $u'$ . However, at lower  $u'$  values, 0.5 m/s,  $u_{tr}$  were observed to flatten beyond  $\phi = 1.1$ .
- (7) Results of  $u_{tr}$ ,  $Ma_{sr}$ , and  $u_{tr}/u_l$  of n-butanol/air mixtures are compared at the same conditions with that of iso-octane/air mixtures.  $u_{tr}$  of n-butanol/air mixtures are higher than iso-octane/air mixtures which is attributed to lower  $Ma_{sr}$ . Moreover, between the two, n-butanol/air flames are observed to possess appreciable burning rates over a range of  $\phi$  studied.
- (8)  $u_{tm}/u'_k$ , derived for n-butanol/air flames are correlated in terms of  $Ma_{sr}$  and  $K$ .  $u_{tm}/u'_k$  values decreased with increasing  $K$  for a given  $Ma_{sr}$ . However, for a constant  $K$ , decrease in  $Ma_{sr}$  lead to increased  $u_{tm}/u'_k$  values.
- (9) The derived values of  $u_{tm}/u'_k$  from present Schlieren measurements are compared with those obtained from previous correlations, and a good agreement is found.
- (10) The  $u_{tm}/u'_k$  curves from the previous studies conducted at Leeds are extended to a positive  $Ma_{sr}$  of 10 along with the quench regime identified.

## Acknowledgements

The authors would like to acknowledge University of Leeds for its support as a Research Scholarship Award to P. Ahmed. The authors would also like to acknowledge the discussions and insights provided by Prof. Derek Bradley and Dr. Malcolm Lawes.

## Disclosure statement

No potential conflict of interest was reported by the author(s).

## References

- Abdel-Gayed, R. G., K. J. Al-Khishali, and D. Bradley 1984. Turbulent burning velocities and flame straining in explosions. *Proceedings of the Royal Society of London. A. Mathematical and Physical Sciences*, vol. 391(1801), 393–414.
- Abdel-Gayed, R. G., D. Bradley, and M. Lawes 1987. Turbulent burning velocities: A general correlation in terms of straining rates. *Proceedings of the Royal Society of London. A. Mathematical and Physical Sciences*, vol. 414(1847), 389–413.
- Alasfour, F. 1997a. Butanol—a single-cylinder engine study: Availability analysis. *Appl. Therm. Eng.* 17 (6):537–49. doi: [10.1016/S1359-4311\(96\)00069-5](https://doi.org/10.1016/S1359-4311(96)00069-5).
- Alasfour, F. 1997b. Butanol—a single cylinder engine study: Engine performance. *Int. J. Energy Res.* 21 (1):21–30. doi: [10.1002/\(SICI\)1099-114X\(199701\)21:1<21::AID-ER231>3.0.CO;2-K](https://doi.org/10.1002/(SICI)1099-114X(199701)21:1<21::AID-ER231>3.0.CO;2-K).
- Aleiferis, P., J. Serras-Pereira, and D. Richardson. 2013. Characterisation of flame development with ethanol, butanol, iso-octane, gasoline and methane in a direct-injection spark-ignition engine. *Fuel* 109:256–78. doi: [10.1016/j.fuel.2012.12.088](https://doi.org/10.1016/j.fuel.2012.12.088).
- Andrew, A.M., 2000. LEVEL SET METHODS AND FAST MARCHING METHODS: EVOLVING INTERFACES IN COMPUTATIONAL GEOMETRY, FLUID MECHANICS, COMPUTER

- VISION, AND MATERIALS SCIENCE, by JA Sethian, Cambridge University Press, Cambridge, UK, 2nd edn. 1999 (first published 1996 as Level Set Methods) xviii+ 420 pp., ISBN (paperback) 0-521-64557-3, (hardback) 0-521-64204-3 (Pbk, £ 18.95). *Robotica*, 18(1), pp.89–92.
- Bagdanavicius, A., P. J. Bowen, D. Bradley, M. Lawes, and M. S. Mansour. 2015. Stretch rate effects and flame surface densities in premixed turbulent combustion up to 1.25 MPa. *Combust. Flame* 162 (11):4158–66. doi: [10.1016/j.combustflame.2015.08.007](https://doi.org/10.1016/j.combustflame.2015.08.007).
- Beatrice, C., C. Bertoli, and N. Giacomo. 1998. New findings on combustion behavior of oxygenated synthetic diesel fuels. *Combust. Sci. Tech.* 137 (1–6):31–50. doi: [10.1080/00102209808952044](https://doi.org/10.1080/00102209808952044).
- Beeckmann, J., Kruse, S., Peters, N. 2010. Effect of ethanol and n-butanol on standard gasoline regarding laminar burning velocities. SAE Tech. Paper 2010-01-1452.
- Beeckmann, J., O. Röhl, and N. Peters. 2009. Numerical and experimental investigation of laminar burning velocities of iso-octane, ethanol and n-butanol. SAE Tech. Paper 2009-01-2784.
- Bhattacharya, T., S. Chatterjee, and T. Mishra. 2004. Performance of a constant speed CI engine on alcohol-diesel microemulsions. *Appl. Eng. Agriculture*. 20 (3):253. doi: [10.13031/2013.16058](https://doi.org/10.13031/2013.16058).
- Bonhomme, A., L. Selle, and T. Poinso. 2013. Curvature and confinement effects for flame speed measurements in laminar spherical and cylindrical flames. *Combust Flame* 160 (7):1208–14. doi: [10.1016/j.combustflame.2013.02.003](https://doi.org/10.1016/j.combustflame.2013.02.003).
- Bradley, D. *How fast can we burn? Symposium (International) on combustion*, 1992. 247–62. Elsevier.
- Bradley, D., P. Gaskell, and X. Gu. 1996. Burning velocities, Markstein lengths, and flame quenching for spherical methane-air flames: A computational study. *Combust Flame* 104 (1–2):176–98. doi: [10.1016/0010-2180\(95\)00115-8](https://doi.org/10.1016/0010-2180(95)00115-8).
- Bradley, D., P. Gaskell, and X. Gu. 1998. The modeling of aerodynamic strain rate and flame curvature effects in premixed turbulent combustion. In *Symposium (International) on Combustion* 27 (1), 849–56. Elsevier.
- Bradley, D., P. Gaskell, X. Gu, and A. Sedaghat. 2005. Premixed flamelet modelling: Factors influencing the turbulent heat release rate source term and the turbulent burning velocity. *Combust Flame* 143 (3):227–45. doi: [10.1016/j.combustflame.2005.05.014](https://doi.org/10.1016/j.combustflame.2005.05.014).
- Bradley, D., M. Haq, R. Hicks, T. Kitagawa, M. Lawes, C. Sheppard, and R. Woolley. 2003. Turbulent burning velocity, burned gas distribution, and associated flame surface definition. *Combust Flame* 133 (4):415–30. doi: [10.1016/S0010-2180\(03\)00039-7](https://doi.org/10.1016/S0010-2180(03)00039-7).
- Bradley, D., R. A. Hicks, M. Lawes, C. G. W. Sheppard, and R. Woolley. 1998. The measurement of laminar burning velocities and Markstein numbers for Iso-octane–air and Iso-octane–n-Heptane–Air mixtures at elevated temperatures and pressures in an explosion Bomb. *Combust Flame* 115 (1–2):126–44. doi: [10.1016/S0010-2180\(97\)00349-0](https://doi.org/10.1016/S0010-2180(97)00349-0).
- Bradley, D., A. Lau, M. Lawes, and F. T. Smith. 1992. Flame stretch rate as a determinant of turbulent burning velocity. *Philos. Trans. Roy. Soc. London A: Mathematical, Physical And Engineering Sciences* 338 (1650):359–87. doi: [10.1098/rsta.1992.0012](https://doi.org/10.1098/rsta.1992.0012).
- Bradley, D., M. Lawes, K. Liu, and M. S. Mansour. 2013. Measurements and correlations of turbulent burning velocities over wide ranges of fuels and elevated pressures. *Proc. Combust. Inst.* 34 (1):1519–26. doi: [10.1016/j.proci.2012.06.060](https://doi.org/10.1016/j.proci.2012.06.060).
- Bradley, D., M. Lawes, K. Liu, S. Verhelst, and R. Woolley. 2007. Laminar burning velocities of lean hydrogen–air mixtures at pressures up to 1.0 MPa. *Combust Flame* 149 (1–2):162–72. doi: [10.1016/j.combustflame.2006.12.002](https://doi.org/10.1016/j.combustflame.2006.12.002).
- Bradley, D., M. Lawes, K. Liu, and R. Woolley. 2007. The quenching of premixed turbulent flames of iso-octane, methane and hydrogen at high pressures. *Proc. Combust. Inst.* 31 (1):1393–400. doi: [10.1016/j.proci.2006.07.022](https://doi.org/10.1016/j.proci.2006.07.022).
- Bradley, D., M. Lawes, and M. Mansour. 2009a. Explosion bomb measurements of ethanol–air laminar gaseous flame characteristics at pressures up to 1.4 MPa. *Combust. Flame* 156 (7):1462–70. doi: [10.1016/j.combustflame.2009.02.007](https://doi.org/10.1016/j.combustflame.2009.02.007).
- Bradley, D., M. Lawes, and M. Mansour. 2009b. Flame surface densities during spherical turbulent flame explosions. *Proc. Combust. Inst.* 32 (1):1587–93. doi: [10.1016/j.proci.2008.06.020](https://doi.org/10.1016/j.proci.2008.06.020).
- Bradley, D., M. Lawes, and M. Mansour. 2011. Measurement of turbulent burning velocities in implosions at high pressures. *Proc. Combust. Inst.* 33 (1):1269–75. doi: [10.1016/j.proci.2010.06.032](https://doi.org/10.1016/j.proci.2010.06.032).

- Bradley, D., M. Lawes, and M. S. Mansour. 2011. Correlation of turbulent burning velocities of ethanol–air, measured in a fan-stirred bomb up to 1.2 MPa. *Combust Flame* 158 (1):123–38. doi: [10.1016/j.combustflame.2010.08.001](https://doi.org/10.1016/j.combustflame.2010.08.001).
- Bradley, D., M. Lawes, and M. Morsy. 2019. Flame speed and particle image velocimetry measurements of laminar burning velocities and Markstein numbers of some hydrocarbons. *Fuel* 243:423–32. doi: [10.1016/j.fuel.2019.01.067](https://doi.org/10.1016/j.fuel.2019.01.067).
- Bradley, D., M. Lawes, and M. Morsy. 2021. Combustion-induced turbulent flow fields in premixed flames. *Fuel* 290:119972. doi: [10.1016/j.fuel.2020.119972](https://doi.org/10.1016/j.fuel.2020.119972).
- Bradley, D., M. Lawes, R. Mumby, and P. Ahmed. 2019. The stability of laminar explosion flames. *Proc. Combust. Inst.* 37 (2):1807–13. doi: [10.1016/j.proci.2018.07.067](https://doi.org/10.1016/j.proci.2018.07.067).
- Bray, K.N.C. January 1996. The challenge of turbulent combustion. In Symposium (International) on combustion 26(01) , 1–26. Elsevier.
- Broustail, G., F. Halter, P. Seers, G. Moréac, and C. Mounaïm-Rousselle. 2013. Experimental determination of laminar burning velocity for butanol/iso-octane and ethanol/iso-octane blends for different initial pressures. *Fuel* 106:310–17.
- Broustail, G., P. Seers, F. Halter, G. Moréac, and C. Mounaïm-Rousselle. 2011. Experimental determination of laminar burning velocity for butanol and ethanol iso-octane blends. *Fuel* 90 (1):1–6. doi: [10.1016/j.fuel.2010.09.021](https://doi.org/10.1016/j.fuel.2010.09.021).
- Chakraborty, N., and R. Cant. 2006. Influence of Lewis number on strain rate effects in turbulent premixed flame propagation. *Int. J. Heat Mass Transf.* 49 (13–14):2158–72. doi: [10.1016/j.ijheatmasstransfer.2005.11.025](https://doi.org/10.1016/j.ijheatmasstransfer.2005.11.025).
- Chen, Z., Z. Wu, J. Liu, and C. Lee. 2014. Combustion and emissions characteristics of high n-butanol/diesel ratio blend in a heavy-duty diesel engine and EGR impact. *Energy Convers. Manag.* 78:787–95. doi: [10.1016/j.enconman.2013.11.037](https://doi.org/10.1016/j.enconman.2013.11.037).
- Chung, K., P. C. Law, M. Mizomoto, and H. Yoshida. 1986. Flame curvature and preferential diffusion in the burning intensity of bunsen flames. *Symp. Int. Combust.* 21 (1):1803–09. doi: [10.1016/S0082-0784\(88\)80414-4](https://doi.org/10.1016/S0082-0784(88)80414-4).
- Clavin, P. 1985. Dynamic behavior of premixed flame fronts in laminar and turbulent flows. *Prog. Energy Combust. Sci.* 11 (1):1–59. doi: [10.1016/0360-1285\(85\)90012-7](https://doi.org/10.1016/0360-1285(85)90012-7).
- Clavin, P., and F. A. Williams. 1982. Effects of molecular diffusion and of thermal expansion on the structure and dynamics of premixed flames in turbulent flows of large scale and low intensity. *J Fluid Mech* 116:251–82. doi: [10.1017/S0022112082000457](https://doi.org/10.1017/S0022112082000457).
- Demirbas, A. 2007. Progress and recent trends in biofuels. *Prog. Energy Combust. Sci.* 33 (1):1–18. doi: [10.1016/j.pecs.2006.06.001](https://doi.org/10.1016/j.pecs.2006.06.001).
- Gautam, M., and D. Martin. 2000. Combustion characteristics of higher-alcohol/gasoline blends. *Proceedings of the Institution of Mechanical Engineers, Part A: Journal of Power and Energy*, 214 (5), 497–511.
- Gautam, M., D. Martin, and D. Carder. 2000. Emissions characteristics of higher alcohol/gasoline blends. *Proc. Inst. Mech. Eng. Part A J. Power Energy* 214 (2):165–82. doi: [10.1243/0957650001538263](https://doi.org/10.1243/0957650001538263).
- Gu, X., Z. Huang, Q. Li, and C. Tang. 2009. Measurements of laminar burning velocities and Markstein lengths of n-butanol– air premixed mixtures at elevated temperatures and pressures. *Energy Fuels* 23 (10):4900–07. doi: [10.1021/ef900378s](https://doi.org/10.1021/ef900378s).
- Gu, X., Z. Huang, S. Wu, and Q. Li. 2010. Laminar burning velocities and flame instabilities of butanol isomers–air mixtures. *Combust. Flame* 157 (12):2318–25. doi: [10.1016/j.combustflame.2010.07.003](https://doi.org/10.1016/j.combustflame.2010.07.003).
- Gu, X. J., M. Z. Haq, M. Lawes, and R. Woolley. 2000. Laminar burning velocity and Markstein lengths of methane–air mixtures. *Combust. Flame* 121 (1–2):41–58. doi: [10.1016/S0010-2180\(99\)00142-X](https://doi.org/10.1016/S0010-2180(99)00142-X).
- Gu, X., Q. Li, and Z. Huang. 2011. Laminar burning characteristics of diluted n-butanol/air mixtures. *Combust. Sci. Tech.* 183 (12):1360–75. doi: [10.1080/00102202.2011.600275](https://doi.org/10.1080/00102202.2011.600275).
- Haq, M., C. Sheppard, R. Woolley, D. Greenhalgh, and R. Lockett. 2002. Wrinkling and curvature of laminar and turbulent premixed flames. *Combust. Flame* 131 (1–2):1–15. doi: [10.1016/S0010-2180\(02\)00383-8](https://doi.org/10.1016/S0010-2180(02)00383-8).

- Karabektas, M., and M. Hosoz. 2009. Performance and emission characteristics of a diesel engine using isobutanol–diesel fuel blends. *Renew. Energy* 34 (6):1554–59. doi: [10.1016/j.renene.2008.11.003](https://doi.org/10.1016/j.renene.2008.11.003).
- Katoch, A., A. Alfazazi, S. M. Sarathy, and S. Kumar. 2019. Experimental and numerical investigations on the laminar burning velocity of n-butanol+ air mixtures at elevated temperatures. *Fuel* 249:36–44. doi: [10.1016/j.fuel.2019.03.047](https://doi.org/10.1016/j.fuel.2019.03.047).
- Kitagawa, T., T. Nakahara, K. Maruyama, K. Kado, A. Hayakawa, and S. Kobayashi. 2008. Turbulent burning velocity of hydrogen–air premixed propagating flames at elevated pressures. *Int. J. Hydrogen Energy* 33 (20):5842–49. doi: [10.1016/j.ijhydene.2008.06.013](https://doi.org/10.1016/j.ijhydene.2008.06.013).
- Kobayashi, H., Y. Kawabata, and K. Maruta January. 1998. Experimental study on general correlation of turbulent burning velocity at high pressure. In Symposium (International) on Combustion 27 (01) , 941–48. Elsevier.
- Kolla, H., J. Rogerson, N. Chakraborty, and N. Swaminathan. 2009. Scalar dissipation rate modeling and its validation. *Combust. Sci. Tech.* 181 (3):518–35. doi: [10.1080/00102200802612419](https://doi.org/10.1080/00102200802612419).
- Kolla, H., J. Rogerson, and N. Swaminathan. 2010. Validation of a turbulent flame speed model across combustion regimes. *Combust. Sci Tech.* 182 (3):284–308. doi: [10.1080/00102200903341587](https://doi.org/10.1080/00102200903341587).
- Konnov, A. 2010. The effect of temperature on the adiabatic laminar burning velocities of CH<sub>4</sub>– air and H<sub>2</sub>– air flames. *Fuel* 89 (9):2211–16. doi: [10.1016/j.fuel.2009.11.038](https://doi.org/10.1016/j.fuel.2009.11.038).
- Lawes, M., M. P. Ormsby, C. G. W. Sheppard, and R. Woolley. 2012. The turbulent burning velocity of iso-octane/air mixtures. *Combust. Flame* 159 (5):1949–59. doi: [10.1016/j.combustflame.2011.12.023](https://doi.org/10.1016/j.combustflame.2011.12.023).
- Lawes, M., M. Ormsby, C. Sheppard, and R. Woolley. 2005. Variation of turbulent burning rate of methane, methanol, and iso-octane air mixtures with equivalence ratio at elevated pressure. *Combust. Sci. Tech.* 177 (7):1273–89. doi: [10.1080/00102200590950467](https://doi.org/10.1080/00102200590950467).
- Li, G., J. Liang, Z. Zhang, L. Tian, Y. Cai, and L. Tian. 2015. Experimental investigation on laminar burning velocities and Markstein lengths of premixed methane–n-Heptane–air mixtures. *Energy Fuels* 29 (7):4549–56. doi: [10.1021/acs.energyfuels.5b00355](https://doi.org/10.1021/acs.energyfuels.5b00355).
- Li, Q., W. Jin, and Z. Huang. 2016. Laminar flame characteristics of C1–C5 primary alcohol–isooctane blends at elevated temperature. *Energies* 9 (7):511. doi: [10.3390/en9070511](https://doi.org/10.3390/en9070511).
- Linan, A., and F. A. Williams. 1993. *Fundamental aspects of combustion*. Oxford, UK: Oxford University Press.
- Lipatnikov, A. N., and J. Chomiak. 2002. Turbulent flame speed and thickness: Phenomenology, evaluation, and application in multi-dimensional simulations. *Prog. Energy Combust. Sci.* 28 (1):1–74. doi: [10.1016/S0360-1285\(01\)00007-7](https://doi.org/10.1016/S0360-1285(01)00007-7).
- Liu, K., J. Fu, B. Deng, J. Yang, Q. Tang, and J. Liu. 2014. The influences of pressure and temperature on laminar flame propagations of n-butanol, iso-octane and their blends. *Energy* 73:703–15. doi: [10.1016/j.energy.2014.06.074](https://doi.org/10.1016/j.energy.2014.06.074).
- Mandilas, C., M. P. Ormsby, C. G. W. Sheppard, and R. Woolley. 2007. Effects of hydrogen addition on laminar and turbulent premixed methane and iso-octane–air flames. *Proc. Combust. Inst.* 31 (1):1443–50. doi: [10.1016/j.proci.2006.07.157](https://doi.org/10.1016/j.proci.2006.07.157).
- Mccomb, W. 1990. *The physics of fluid turbulence*. Oxford University Press: Oxford.
- Merola, S. S., C. Tornatore, G. Valentino, L. Marchitto, and F. Corcione. 2011. Optical investigation of the effect on the combustion process of butanol-gasoline blend in a PFI SI boosted engine. SAE Technical Paper.
- Morley, C. 2005. Gaseq: A chemical equilibrium program for Windows, Ver. 0.79.
- Morsy, M. E. M. H. 2019. *Studies of laminar and turbulent combustion using particle image velocimetry*. Doctoral dissertation: University of Leeds.
- Nwagwe, I. K., H. G. Weller, G. R. Tabor, A. D. Gosman, M. Lawes, C. G. W. Sheppard, and R. Wooley. 2000. Measurements and large eddy simulations of turbulent premixed flame kernel growth. *Proc. Combust. Inst.* 28 (1):59–65. doi: [10.1016/S0082-0784\(00\)80195-2](https://doi.org/10.1016/S0082-0784(00)80195-2).
- Oecd, F. 2011. *OECD-FAO Agricultural Outlook 2011–2020*. Paris, France: Organisation for Economic Co-operation and Development (OECD) Publishing.
- Qin, X., and Y. Ju. 2005. Measurements of burning velocities of dimethyl ether and air premixed flames at elevated pressures. *Proc. Combust. Inst.* 30 (1):233–40. doi: [10.1016/j.proci.2004.08.251](https://doi.org/10.1016/j.proci.2004.08.251).

- Ranzi, E., A. Frassoldati, R. Grana, A. Cuoci, T. Faravelli, A. P. Kelley, and C. K. Law. 2012. Hierarchical and comparative kinetic modeling of laminar flame speeds of hydrocarbon and oxygenated fuels. *Prog. Energy Combust. Sci.* 38 (4):468–501. doi: [10.1016/j.pecs.2012.03.004](https://doi.org/10.1016/j.pecs.2012.03.004).
- Sarathy, S., M. Thomson, C. Togbé, P. Dagaut, F. Halter, and C. Mounaim-Rousselle. 2009. An experimental and kinetic modeling study of n-butanol combustion. *Combust Flame* 156 (4):852–64. doi: [10.1016/j.combustflame.2008.11.019](https://doi.org/10.1016/j.combustflame.2008.11.019).
- Serras-Pereira, J., P. Aleiferis, and D. Richardson. 2013. An analysis of the combustion behavior of ethanol, butanol, iso-octane, gasoline, and methane in a direct-injection spark-ignition research engine. *Combust. Sci. Tech.* 185 (3):484–513. doi: [10.1080/00102202.2012.728650](https://doi.org/10.1080/00102202.2012.728650).
- Shepherd, I., and R. Cheng. 2001. The burning rate of premixed flames in moderate and intense turbulence. *Combust Flame* 127 (3):2066–75. doi: [10.1016/S0010-2180\(01\)00309-1](https://doi.org/10.1016/S0010-2180(01)00309-1).
- Simon, D. M. 1951. Flame propagation. III. Theoretical consideration of the burning velocities of Hydrocarbons1. *J. Am Chem. Soc* 73 (1):422–25. doi: [10.1021/ja01145a137](https://doi.org/10.1021/ja01145a137).
- Siwale, L., L. Kristóf, T. Adam, A. Bereczky, M. Mbarawa, A. Penninger, and A. Kolesnikov. 2013. Combustion and emission characteristics of n-butanol/diesel fuel blend in a turbo-charged compression ignition engine. *Fuel* 107:409–18. doi: [10.1016/j.fuel.2012.11.083](https://doi.org/10.1016/j.fuel.2012.11.083).
- Szwaja, S., and J. Naber. 2010. Combustion of n-butanol in a spark-ignition IC engine. *Fuel* 89 (7):1573–82. doi: [10.1016/j.fuel.2009.08.043](https://doi.org/10.1016/j.fuel.2009.08.043).
- Tripathi, N. 2012. *Dynamics of confined premixed laminar explosion flames*. Doctoral dissertation: University of Leeds.
- Valentino, G., F. E. Corcione, S. E. Iannuzzi, and S. Serra 2012. Experimental study on performance and emissions of a high speed diesel engine fuelled with n-butanol diesel blends under premixed low temperature combustion. *Fuel* 92:295–307.
- Van Lipzig, J. P. J., E. J. K. Nilsson, L. P. H. De Goey, and A. A. Konnov. 2011. Laminar burning velocities of n-heptane, iso-octane, ethanol and their binary and tertiary mixtures. *Fuel* 90 (8):2773–81. doi: [10.1016/j.fuel.2011.04.029](https://doi.org/10.1016/j.fuel.2011.04.029).
- Veloo, P. S., and F. N. Egolfopoulos. 2011. Flame propagation of butanol isomers/air mixtures. *Proc. Combust. Inst.* 33 (1):987–93. doi: [10.1016/j.proci.2010.06.163](https://doi.org/10.1016/j.proci.2010.06.163).
- Veloo, P. S., Y. L. Wang, F. N. Egolfopoulos, and C. K. Westbrook. 2010. A comparative experimental and computational study of methanol, ethanol, and n-butanol flames. *Combust Flame* 157 (10):1989–2004. doi: [10.1016/j.combustflame.2010.04.001](https://doi.org/10.1016/j.combustflame.2010.04.001).
- Wang, G., Y. Li, W. Yuan, Y. Wang, Z. Zhou, Y. Liu, and J. Cai. 2018. Investigation on laminar flame propagation of n-butanol/air and n-butanol/O<sub>2</sub>/He mixtures at pressures up to 20 atm. *Combust. Flame* 191:368–80. doi: [10.1016/j.combustflame.2018.01.025](https://doi.org/10.1016/j.combustflame.2018.01.025).
- Wu, F., and C. K. Law. 2013. An experimental and mechanistic study on the laminar flame speed, Markstein length and flame chemistry of the butanol isomers. *Combust. Flame* 160 (12):2744–56. doi: [10.1016/j.combustflame.2013.06.015](https://doi.org/10.1016/j.combustflame.2013.06.015).
- Yacoub, Y., R. Bata, and M. Gautam. 1998. The performance and emission characteristics of C1-C5 alcohol-gasoline blends with matched oxygen content in a single-cylinder spark ignition engine. *Proc. Inst. Mech. Eng. Part A J. Power Energy* 212 (5):363–79. doi: [10.1243/0957650981536934](https://doi.org/10.1243/0957650981536934).
- Yao, M., H. Wang, Z. Zheng, and Y. Yue 2010. Experimental study of n-butanol additive and multi-injection on HD diesel engine performance and emissions. *Fuel* 89:2191–201.
- Zhang, X., C. Tang, H. Yu, Q. Li, J. Gong, and Z. Huang 2013. Laminar flame characteristics of iso-octane/n-butanol blend–air mixtures at elevated temperatures. *Energy & Fuels* 27:2327–35.
- Zhang, Z., Z. Huang, X. Wang, J. Xiang, X. Wang, and H. Miao. 2008. Measurements of laminar burning velocities and Markstein lengths for methanol–air–nitrogen mixtures at elevated pressures and temperatures. *Combust. Flame* 155 (3):358–68. doi: [10.1016/j.combustflame.2008.07.005](https://doi.org/10.1016/j.combustflame.2008.07.005).
- Zhang, Z., S. Zhu, J. Liang, L. Tian, and G. Li. 2018. Experimental and kinetic studies of premixed laminar flame of acetone-butanol-ethanol (Abe)/air. *Fuel* 211:95–101. doi: [10.1016/j.fuel.2017.09.063](https://doi.org/10.1016/j.fuel.2017.09.063).

## Appendix

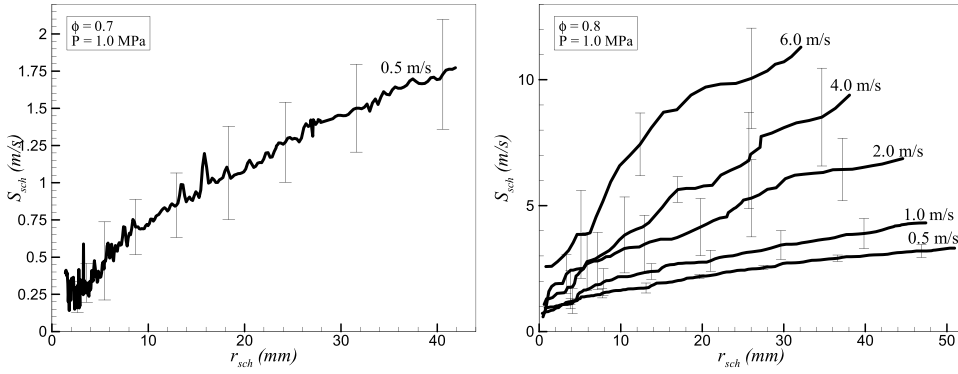


**Figure A1.** Variation of  $S_{sch}$  with increasing radii from ignition for different  $u'$  at  $\phi = 0.7, 0.8$  at 1.0 MPa, 360 K.

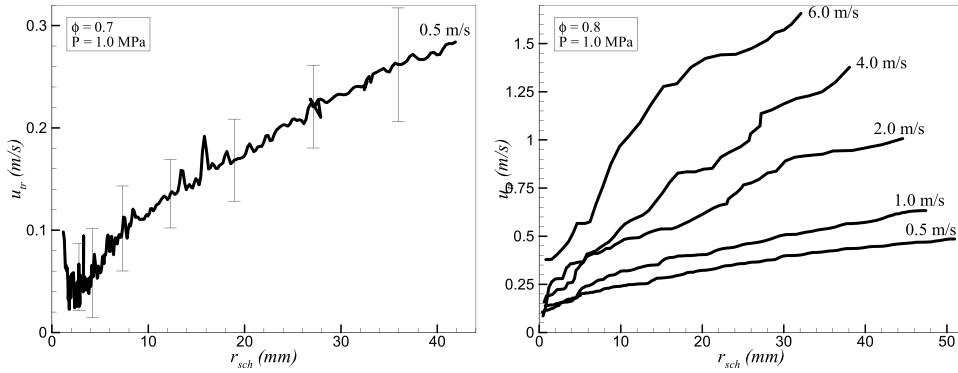


**Figure B1.** Variation of  $u_{tr}$  with increasing radii from ignition for different  $u'$  at  $\phi = 0.7, 0.8$  at 1.0 MPa, 360 K.

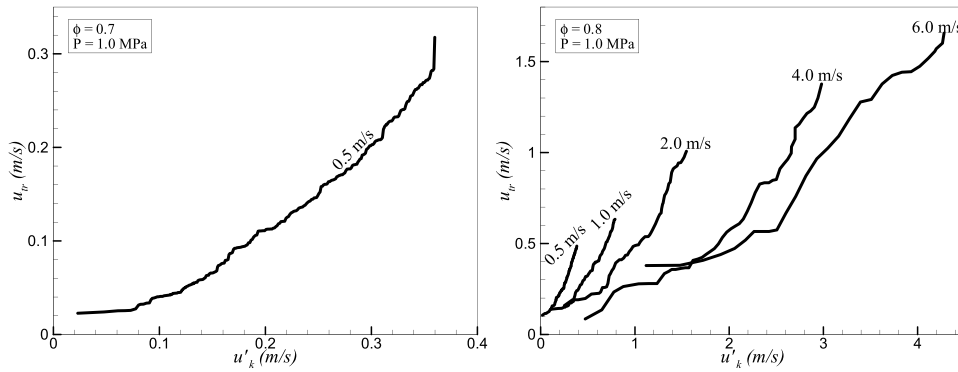


**Figure C1.** Variation of  $u_{tr}$  with  $u'_k$  for different  $u'$  at  $\phi = 0.7, 0.8$  at 1.0 MPa, 360 K.